MICROELECTRIC DISCHARGE MACHINING SPINDLE DESIGN

by

Thomas James Ross

A thesis submitted to the faculty of
The University of Utah
in partial fulfillment of the requirements for the degree of

Master of Science

Department of Mechanical Engineering

The University of Utah

December 2014

The University of Utah Graduate School

STATEMENT OF THESIS APPROVAL

The thesis of **Thomas James Ross**

has been approved by the following supervisory committee members:

Eberhard Bamberg	, Chair	**12/11/2013** Date Approved
Alagar Krishnan Balaji	, Member	**12/11/2013** Date Approved
Donald Bloswick	, Member	**12/11/2013** Date Approved

and by **Tim Ameel** , Chair/Dean of

the Department/College/School of **Mechanical Engineering**

and by David B. Kieda, Dean of The Graduate School.

ABSTRACT

Technological advancements have created a demand for ever more complex components with extremely small features, high aspect ratios, and tight tolerances. Components are also being made from harder materials, which are more difficult to produce with traditional machining methods. Electric discharge machining (EDM) offers a manufacturing method that addresses these issues. Micro electric discharge milling is a powerful method that rotates the electrode and enables the cutting of complex 3-D pockets with standard electrodes.

In order to meet some of the challenges in the micro manufacturing industry, an micro electric discharge milling spindle has been designed. This design uses a standard industrial collet, is capable of loading a large variety of electrode sizes and shapes, and incorporates optimal dielectric flushing. The spindle design offers injection flushing through the electrode and side flushing for the use of solid electrodes. This spindle design also offers the unique feature of variable flushing pressure. The spindle varies the injection pressure automatically to maintain a constant flow rate of dielectric fluid through the electrode as the electrode becomes shorter. The spindle is also capable of automatically feeding and fixturing the electrode as it wears down. The addition of a C-axis gives the spindle the unique ability to rotationally orient the tool. When the C-axis ability of the spindle is used in conjunction with wire electric discharge grinding, the machine is given the ability to produce a large variety of electrode shapes with extremely

high aspect ratios and small features.

This spindle design offers an economical versatile and compact solution to micro-electric discharge milling and can be easily placed into a CNC machine platform for accurate creation of complex features. The electrode fixturing range, variable dielectric pressure, and C-axis capabilities of this design are unique to this design and are not offered on the current market.

TABLE OF CONTENTS

CHAPTER 1

INTRODUCTION

1.1 Current Challenges in Micromachining

Micromachining is in high demand in the manufacturing industry due to the technological advancements in the medical, aerospace, automotive, molding, and optical equipment. Today's advanced machinery utilizes components made from a range of exotic materials capable of increased mechanical properties, which allow mechanisms to operate in environments beyond the scope of traditional materials. These materials also present challenges to the manufacturing methods used to process them. In addition to the materials becoming more difficult to process, the component features are becoming ever more complex. Smaller features with higher aspect ratios, tighter tolerances, and improved surface quality are in demand in the manufacturing industry, yet many of the traditional manufacturing methods are not capable of meeting these demands.

1.2 The Electric Discharge Milling Overview

The electric discharge machining (EDM) process is suitable for being down sized into the micro scale and is capable of achieving features with remarkable complexity at higher aspect ratios and accuracies. The EDM process is also capable of cutting very hard materials. Since the EDM process produces no significant cutting forces the method is ideal for creating features with high aspect ratios and high accuracy. The EDM process

is also well suited for components where thermal warping of the part produces accuracy challenges. While the EDM process is a thermal one, the presence of the dielectric fluid and relatively slow material removal rates allows the workpiece to remain thermally stable during the process.

EDM machining has become regarded as a traditional machining method in the micro scale. Electric discharge milling machines are widely used in the creation of micro molds, micro dies, and complex 3D cavities in hard-to-machine materials [1]. Small hole EDM machining is also a widely used method in the production of turbine blades, spinnerets, and starter holes for a wire EDM. Having a machine center capable of performing both electric discharge milling and small hole drilling provides a high degree of versatility in a compact platform.

The electric discharge milling process utilizes a rotating electrode to perform electrical discharge to the workpiece. The rotation produces more even wear of the electrode and enhances flushing [2]. This type of EDM configuration allows for three dimensional tool paths to be executed much like a traditional vertical CNC milling machine. Figure 1.1 depicts how this is done on an electric discharge mill by removing one layer at a time. The electric discharge milling process enables the use of tool path orbiting and servo motion in multiple axes to aid in cutting efficiency and performance. The process is capable of producing complex features with standard economical electrodes, unlike a sinker EDM which requires customized electrodes for each feature to be cut. An electric discharge mill is also capable of performing Z axis plunging much like a sinker EDM and enables the machining platform to perform deep hole drilling.

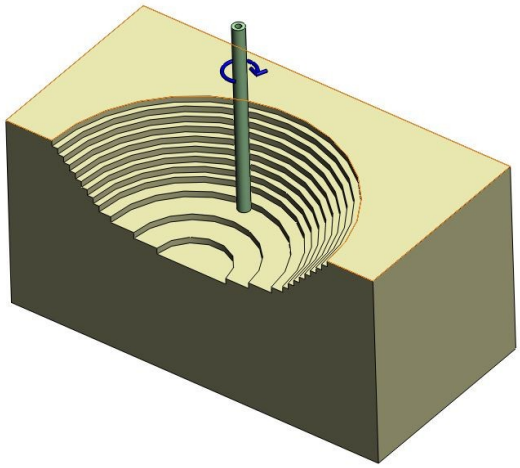

Figure 1.1: Electric discharge milling schematic

1.3 WEDG

Another advantage to rotating the electrode is the ability to employ wire electric discharge grinding (WEDG). This method was first developed by Masuzawa [3] in 1985 and has proven to be a useful tool in the creation of electrode tooling that is slender with extremely high aspect ratios [4]. This method involves the use of a system similar to a wire EDM which continuously pulls a small diameter wire for discharging to the electrode. In the WEDG method the rotating electrode is positioned next to the wire so that discharging provides shaping of the electrode. This method is depicted in Figure 1.2. Using the WEDG method electrodes can be reduced to diameters as small as 5µm, which is extremely difficult to accomplish using any other method [5]. The WEDG method also improves run out accuracy by negating the effects of nonconcentric chucking of the electrode. Using this method can also provide an accurate height offset for the electrode if WEDM is used to cut the electrode to length. This is a significant advantage in the use of microelectrodes due to the difficulty of chucking concentricity and the detection of the

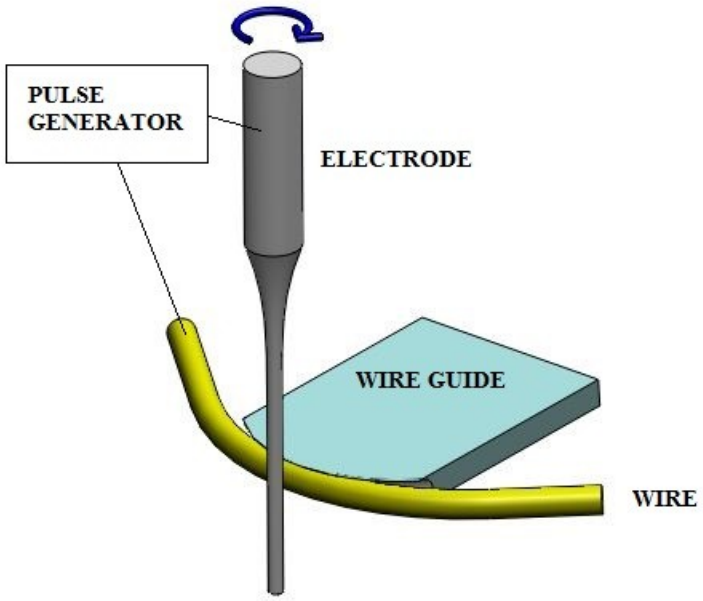

Figure 1.2: WEDG schematic

extremely fragile electrode. The WEDG unit can also be used to create cutting tools and is considered the most useful EDM method in the production of micro milling tools [6].

If the EDM spindle used can support the speed and rigidity requirements of high speed micro machining, then a tool can be created using WEDG and then moved to cut the workpiece without rechucking. In addition to creating cutting tools, the method has been shown to be successful in the creation of micro probes [7]. Using the WEDG unit to create tooling is a significant asset considering the limited availability of micro-tools [8].

Wear of the electrode occurs during the EDM process and causes inaccuracies in the created features. Length compensation methods, such as pulse monitoring, can be used to improve accuracy; however, it is difficult to anticipate wear unless the material and cutting conditions are well known [9]. Using the WEDG method, the electrode can be dressed periodically to a known height. The geometry of the electrode is also an

important factor in the effect of wear. A tubular electrode minimizes the rounding off of the bottom of the tool and allows for the wear to be concentrated at the bottom face of the tool where only Z level compensation is required. The tubular electrode is also easy to refresh by simply parting off the bottom of the electrode using the WEDG method.

1.4 Dielectric Fluids

In the EDM process the choice of dielectric fluid and its method of flushing are of critical importance. Dielectric fluid performs in three ways: it is a conductive barrier so that sufficient energy can build up in the discharge gap; it is a cooling medium to help solidify the recast material after discharging; and it is used to transport the recast material from the discharge gap through flushing. Generally, the dielectric fluid is kerosene or deionized water. The choice of fluid is important as it affects material removal rate, electrode wear, surface finish, and the composition of the recast layer. Important characteristics of the dielectric fluid include the viscosity, ionization point, toxicity and thermal conductivity.

Though there are benefits to using either kerosene or deionized water, water seems to be a better overall choice. In micro electric discharge milling, the use of deionized water produces significantly higher material removal rates compared to kerosene [1,10,11,12]. The discharge gap when using deionized water is larger than that found using kerosene [10]. This results in kerosene being able to produce finer cuts with the same electrode. However, when kerosene is used, carbon is released during the discharging which contaminates the recast layer [1,12]. This high carbon content creates an extremely hard surface with a larger heat affected zone. When using deionized water there is no carbon released. Instead, hydrogen diffuses into the heat affected zone,

thereby creating a white layer with reduced thickness [4]. In some cases, it can produce a smoother surface finish than kerosene [1,10,12].

Another problem with using kerosene is that harmful vapors, such as CO and CH_4, are produced. In comparison, "deionized water promotes a better and safer machining environment" [12]. Deionized water also has the clear safety advantage of not being flammable. Since the EDM process involves arcing, it is important to consider the hazards of using a flammable dielectric fluid.

Kerosene also quickly degrades many of the materials used for seals built into the EDM machine and the seals used in the compressor, regulator, and filtration systems [13]. Deionized water is corrosive to the metal components by causing oxidation but this problem is easier to handle. Also, using deionized water in many cases results in less electrode wear [1,10,11].

Deionized water does require more routine maintenance than kerosene as its dielectric properties degrade, and the fluid is easily contaminated [14]. As a result, the water needs to be continuously retreated and filtered. Deionized water also "cracks" and releases hydrogen at the discharge [15]. When machining materials with a high affinity for hydrogen, the surface may suffer from hydrogen embrittlement. Deionized water will also release oxides when vaporized with the workpiece, making it difficult to perform skim cuts due to increased resistance of the oxidized surface [15].

Despite increased routine maintenance and possible issues due to released hydrogen, deionized water is preferred to kerosene for the following reasons: it provides a much higher material removal rate than kerosene while producing a thinner martensite layer and softer surface; it is safer for the machine and the operator; and deionized water

has a lower viscosity than oil, making it possible to inject dielectric fluid through small holes and gaps.

1.5 Flushing in the EDM Process

A critically important factor in the EDM process is the flushing [15]. A common saying among EDM machinists is, "There are three rules for successful EDMing: flushing, flushing, and flushing." [16]. A buildup of EDM debris in the discharge gap causes shorting and reduces the machining efficiency. EDM debris concentrated along the side of the electrode will cause secondary discharging causing oversized features, a poor surface finish, and side wear of the electrode. Flushing is required to clear the debris and replenish fresh dielectric in discharge gap. The options for flushing consist of suction, side, injection, and immersion flushing.

Suction flushing is extremely effective because the dielectric fluid is pulled away from the discharge gap rather than being forced through it. Suction flushing requires a path running through the part, making it impossible to use in blind holes and pockets. Since very few features meet this requirement, suction flushing is not commonly used.

Side flushing consists of directing a stream of dielectric to the electrode through nozzles. Side flushing is the least effective form of flushing. Side flushing can cause damage to the workpiece and deflection of the electrode. Side flushing does not effectively project dielectric fluid and EDM debris out of the cavity and has been found to be unsuitable in deep hole drilling [17]. Side flushing is, however, the most versatile flushing method as it does not require a path through the electrode or the workpiece. Injection flushing consists of dielectric fluid being forced through the center of the electrode. The dielectric fluid escapes the machined cavity through the discharge

gap, allowing the evacuation of EDM debris. Injection flushing is the preferred and most common method of flushing [16]. Injection flushing has been shown to yield significantly higher material removal rates than side flushing by keeping discharge material clear from the electrode [2]. Injection flushing is effective even in deep hole drilling where flushing is the most difficult. This is due to the fact that the dielectric fluid escapes the tip of the electrode and provides flushing even when in deep holes. Experimental results show that EDM drilling using through tube injection rather than a solid electrode yields lower electrode wear and a better surface finish [18]. A tube is a natural choice in injection flushing because it provides a path through the electrode and minimizes the rounding off of the bottom of the electrode. A tubular electrode is also an industry standard and is available in a large variety of sizes and materials. High pressure dielectric fluid running through the center of a tube has a stiffening effect, so as the fluid exits the hole, it tends to center the electrode [16]. Studies have shown that as the pressure into the tube is increased, the material removal rate is also increased up until 580 psi [19].

Immersion flushing is obtained by performing the discharging while submerged in the dielectric fluid. The immersion method is the most gentle on the workpiece and suitable for cutting features that may break off using other methods. The immersion method yields a small overcut and can be combined with other flushing methods [17].

Rotation of the electrode is another way to enhance flushing while resulting in even tool wear. Increasing the electrode rotational speed increases the material removal rate and decreases the surface roughness [18]. The centripetal forces generated through electrode rotation aids in ejecting debris from the interface between the workpiece and

the tool [20]. Rotational speed has an even more significant effect in micro EDM machining whenever the current is low and the debris is finer [21].

CHAPTER 2

PROPOSED SPINDLE DESIGN ADVANTAGES

2.1 List of Objectives

There is a demand in the micromachining industry for an EDM spindle that is compact and can be easily configured into a CNC machine platform. It is proposed that an EDM spindle be designed that meets the following objectives:

- Low run out fixturing of standard electrode sizes from 250μm diameter and up
- Automatic feed of the electrode with electrode length detection
- Provide discharge voltage to the electrode
- Variable injection flushing
- Electrode rotation with C-axis capability
- Easy and accurate assembly

The proposed spindle design focuses on flushing and the ability to handle very small diameter electrodes accurately. The following subsections detail a few of the above mentioned features. Figure 2.1 provides a cross section view of the spindle and an overview of the design which points out some of the major components of the design.

2.2 Low Run Out Electrode Fixturing of Standard Electrode Sizes

The spindle design utilizes the standard 1C collet to fixture the electrode. The 1C collet was chosen for the simplicity and versatility it brings to fixturing the electrode. The

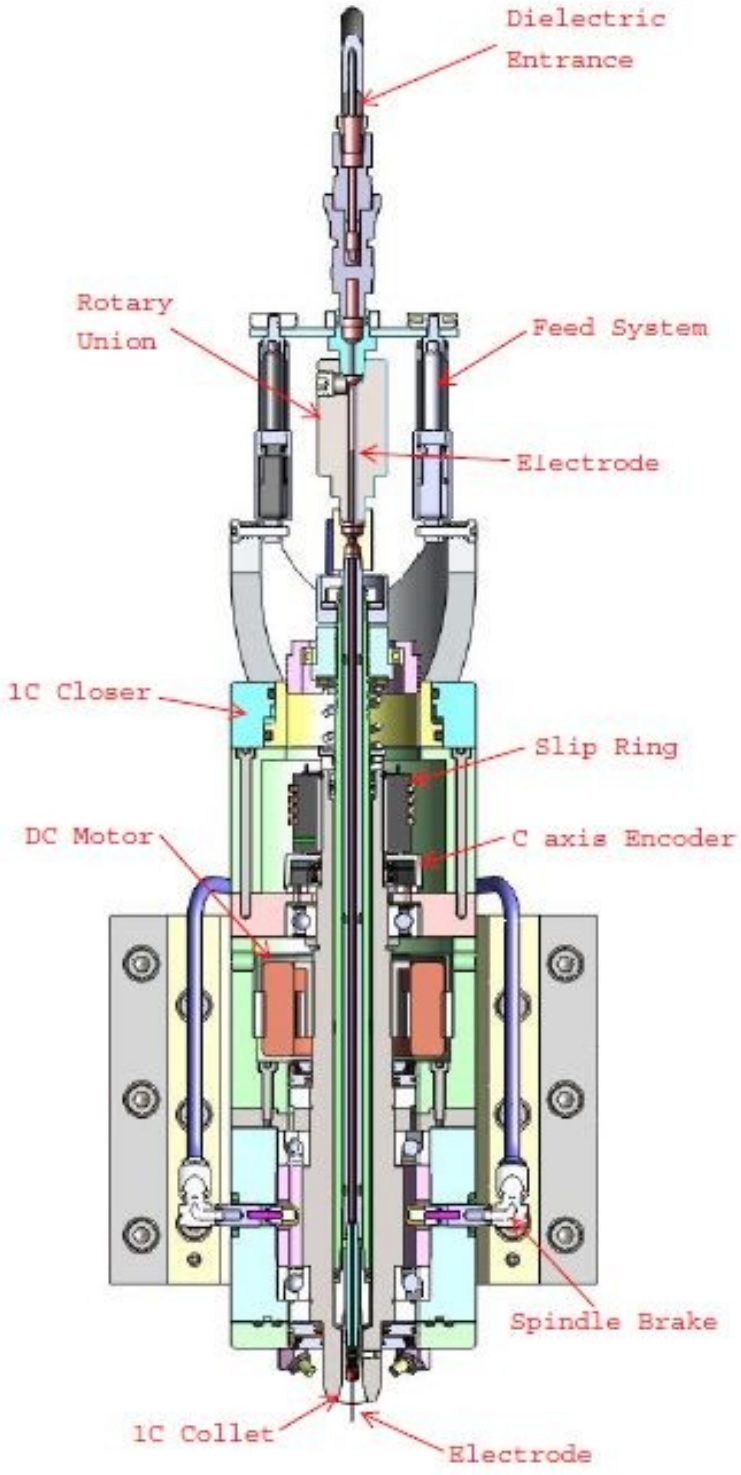

Figure 2.1: Design overview

1C collet has a pull-back design that is reliable and repeatable. The draw force is passive and adjustable from 0 to 370 N. The 1C collet is available as standard from a diameter of 0.25mm to 6.35mm. The 1C collet also comes standard in round, hex, or square shapes. The 1C collet is readily available, economical and easy to install when changing electrode sizes. The collet comes standard with a total indicator run out of less than 7µm. The use of the 1C collet is unique to this electric discharge machining spindle design.

The 1C collet is closed with a spring and released with pneumatic pressure which is released from the chamber through a 3 way valve when closing the collet. The closing force is varied by adjusting the preload on the closing spring. This custom closer design is integrated into the spindle providing a cancellation of the closing force through the spindle shaft. This is a significant advantage as it greatly reduces the amount of load seen by the precision spindle bearings leading to longer bearing life and increased performance.

2.3 Automatic Feeding of Electrode with Electrode Length Detection

As the electrode wears down it needs to be advanced to provide the desired electrode length. This feeding motion is obtained using two Firgelli linear actuators and a microgripper design. The linear actuators are in a closed loop with the controller allowing for tracking of the electrode's length. This length can then be updated to the hydraulic regulator to maintain a constant exit velocity of the dielectric fluid. The actuators can extend the electrode at programmable length up to 10mm per stroke. The actuator can complete the stroke cycle in less than one second and has a positional accuracy of 0.10mm. The Firgelli L12 series actuator is a standard item that provides an economical and compact solution to electrode feeding. The actuators are easy to access

and install for service or replacement.

The microgripper design allows for grasping the electrode within 14mm of the face of the 1C collet. The unique gripper design uses the hydraulic system that is already in place for injecting dielectric fluid. The gripper is hydraulically closed and spring opened. This design gives the machine controller the ability to open the gripper by releasing the hydraulic pressure out of the spindle through a three way valve that drains to the reservoir tank.

2.4 Discharge Voltage to Electrode

The spindle achieves electrical contact to the rotating spindle shaft through the SR-002 slip ring made by Rotary Systems. This component allows for 30 amps to be provided to the electrode. The slip ring is also used to provide the machine controller feedback for electrode detection. The electrode completes an electrical path between the spindle shaft and microgripper. The microgripper loses contact with the electrode as the electrode becomes less than 14mm long. This loss of contact informs the controller to stop machining and allows the operator to load a new electrode.

2.5 Variable Injection Flushing

At the heart of the spindle design is flushing. The spindle provides up to 1000 psi for injecting dielectric fluid through electrode tubing. The spindle is also fitted with four nose jets to provide side flushing. The nose jets are also high pressure and located at optimal locations for access to the electrode. The spindle is designed to be able to reach into a tank so that immersion flushing can easily be employed.

The spindle is capable of loading 400 mm long electrode tubing and machining it

down to 14 mm. As the tube's length is shortened the exit velocity of the dielectric fluid will increase drastically due to the decrease in drag from the narrow inner diameter of the electrode. In order to optimize the EDM process the exit velocity of the dielectric needs to be controlled and held constant. The spindle design incorporates a high pressure regulator with an electro-pneumatic controller. This unique design gives the machine the ability to decrease the injection pressure as the electrode shortens, providing a constant exit velocity. The machine can be programmed to determine an appropriate injection pressure based on the length and inner diameter of the electrode. This allows for the machine operator to simply input the length and inner diameter of the loaded electrode and the desired exit velocity. The machine will then determine an appropriate injection pressure. This feature is unique to this design and offers unparalleled control of the injection flushing process.

2.6 Electrode Rotation with C-axis Capability

The spindle design incorporates a frameless brushless DC servo motor capable of speeds of up to 1700 rpm. The motor's frameless design allows for the rotor to be mounted directly to the spindle eliminating the need to transmit the torque from an off axis motor. This configuration is compact by keeping the motor in line with the spindle.

The servo motor is used in conjunction with an optical encoder to allow C-axis control of the spindle. This capability allows for orientation of the electrode. The spindle is given this ability so that when used with a WEDG unit a variety of different electrode shapes can be produced. Using this method, electrode shapes such as polygons can be cut without the need for re-fixturing the electrode. Being able to shape the electrode in this way allows for microhex sockets or microslits to be cut by using the

custom electrode to plunge in the Z-axis much like a sinker EDM. The electrode's position may be determined before shaping on the WEDG unit. Touching the tool off prior to shaping is a significant advantage due to difficulty of determining the position of the small features created using the WEDG unit. Not only is the tool's length already known but the machine also knows the orientation of the electrode, allowing accurate placement of the cut in the workpiece. A pneumatic spindle brake is another feature of the C-axis. The brake is designed to eliminate servo dithering while creating the electrode or sinking the feature. This design promotes more accurate positioning and less heat generation from the motor. The use of a full C-axis used in conjunction with spindle brakes is unique to this design.

2.7 Easy and Accurate Assembly

Ease and accuracy of the assembly process is part of the spindle design, and assembly tools have been designed to aid in pressing the precision bearings. The pressing tools ensure that the correct race of the bearing loaded to achieve the pressing force. This is an important detail as incorrect loading of the bearing races will result in high loads passing through the ceramic rolling elements that cause permanent damage to the bearing. This EDM spindle is designed to be economical as it has few complex components. The tolerances chosen for each part reflects the functional requirements for each component, allowing for economical manufacturing. The components are designed in such a way that standard machine fixturing and tooling can be used to produce each part. The precision components such as the spindle shaft or the spindle housing are designed so that the critical bearing contact surfaces can be ground in a cylindrical

grinding machine in one setup. This promotes optimal concentricity of the surfaces by eliminating the errors associated with re-chucking.

The spindle has an alignment fixture incorporated into its design to allow accurate placement of the spindle into a machine platform. Using this fixture the spindle's rotational axis can be aligned orthogonally with the machine's positional X, Y, and Z axes. The spindle housing is mounted to a precision V-block to ensure minimal deformation of the spindle. The fixture design includes two flexures which are used to precisely adjust the pitch of the spindle to align with the Z-axis of the machining center. A precision dowel pin is pressed into the mounting plate to allow for easy yaw adjustment of the spindle.

The spindle is configured with the option of adding a ceramic guide and holder for deep hole drilling. This simple feature enables the spindle create much deeper small holes with minimal whipping of the electrode. Adding the WEDG unit and deep hole drilling guide provides the machine platform with incredible versatility. The spindle is then capable using a wide range of standard sized electrodes to produce a variety of cut features. The WEDG unit and C-axis allow the spindle to create customized electrodes of various shapes which the spindle can then use much like a sinker EDM. The deep hole guide provides the ability to load long electrodes and to inject dielectric through the electrode. This allows the spindle to be used like a deep hole popper in addition to its primary purpose of being an electric discharge mill.

The spindle design is capable of injecting dielectric through electrodes up to 400 mm in length. In order to obtain optimal accuracy in the spindle the components are designed around the manufacturing methods and tooling used to produce them. The

spindle is designed for longevity using ceramic rolling elements in spindle bearings and hardened stainless steel for the spindle shaft and housing.

CHAPTER 3

SPINDLE DESIGN OVERVIEW

3.1 Rotary Union

One of the challenges to through spindle dielectric flow is the ability to pass pressurized fluid into a rotating tube. The current design addresses this issue with the use of a rotary union. A rotary union was chosen over a sealed bearing or lip seal design due its low rotational drag. A rotary union accomplishes this by pressing two flat surfaces together using a spring to maintain loaded contact. The surfaces pressed together are lapped to achieve higher degree of flatness and smooth surface finish. Common material choices for stationary and rotating surfaces include silicon carbide, ceramic, tungsten carbide and carbon [22]. This type of seal is known as a mechanical seal and it is common in pumps and compressors. Figure 3.1 is a depiction of the mechanical seal used. The rotary union used in the spindle design is the Series 008 High Speed Air/Hydraulic Rotary Union made by Rotary Systems. This union allows a rotational speed of 1000 rpm while sealing 1000 psi of hydraulic pressure.

3.2 Dielectric Fluid Path

The fluid path of dielectric into the electrode starts at the hydraulic pump. The hydraulic pump selected can produce a pressure of up to 1800 psi while providing 8.1 gallons per minute to the system. The dielectric then passes into the filtration system

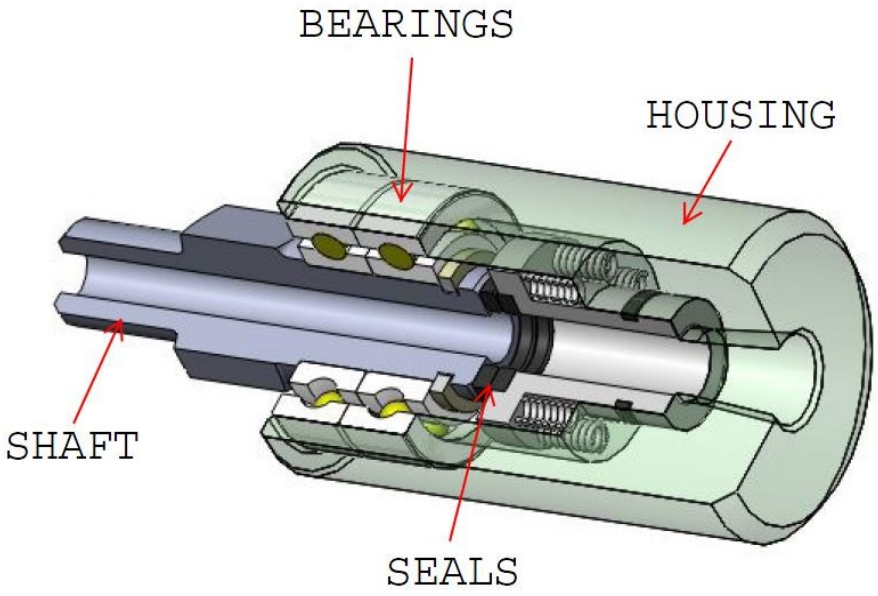

Figure 3.1: Mechanical seal [Adapted from 23]

which maintains the quality and purity of the deionized water.

The dielectric then flows into the regulator system. The regulator system is automatically adjusted by the machine's controller. This is done by using the Tescom ER3P kit [24]. This enclosed unit includes the ER3000 series electro-pneumatic controller which is used to control Tescom's 2600-20 supply regulator. The 2600-20 is capable reducing a 10,000 psi inlet pressure to a 0-1500 psi output. The kit also includes an outlet transducer, a pneumatic regulator, and a junction box assembled into a case. Figure 3.2 shows a schematic of the system layout.

After leaving the regulator system the dielectric feeds into the spindle through the Swagelok SS Instrumentation Quick-Connect. This allows easy assembly when changing the electrode. The fluid path then flows through the rotary union and enters the feed tube. The feed tube is capped off by the micro closer forcing the dielectric to exit the feed tube

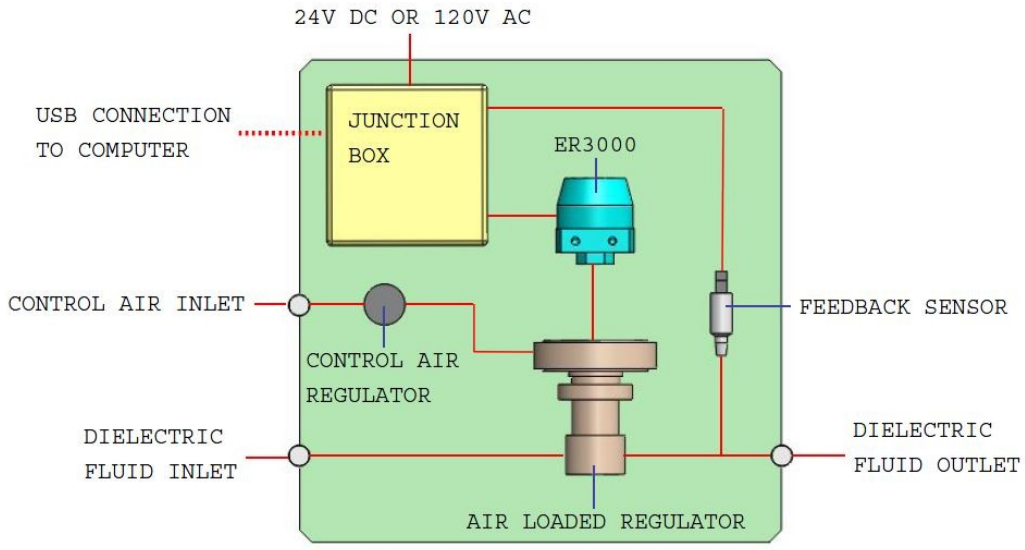

Figure 3.2: Schematic of Tescom ER3P kit [Adapted from 24]

through the electrode. After exiting the electrode the dielectric collects in the machines tank and drains back into the pump's reservoir. Figure 3.3 depicts a cross section of the upper portion of the spindle where the dielectric enters.

The alternative fluid path to the nose jets also begins at hydraulic pump but then diverts away from the Tescom regulator system show in Figure 3.2 and enters into the manually adjusted pressure regulator and metering valve. The regulator used in the current design is the Swagelok SS Compact Regulator and the valve used is from Alta Robbins. This regulator controls the pressure to nose jets from 0 to 1000 psi.

Components can be manufactured from this material using standard metal working tools and methods. This design eliminates the need for additional components to be added to perform electrical insulation. Having fewer components increases simplicity and decreases the overall size of the spindle.

The electrical path includes an entrance for the discharge voltage into the spindle

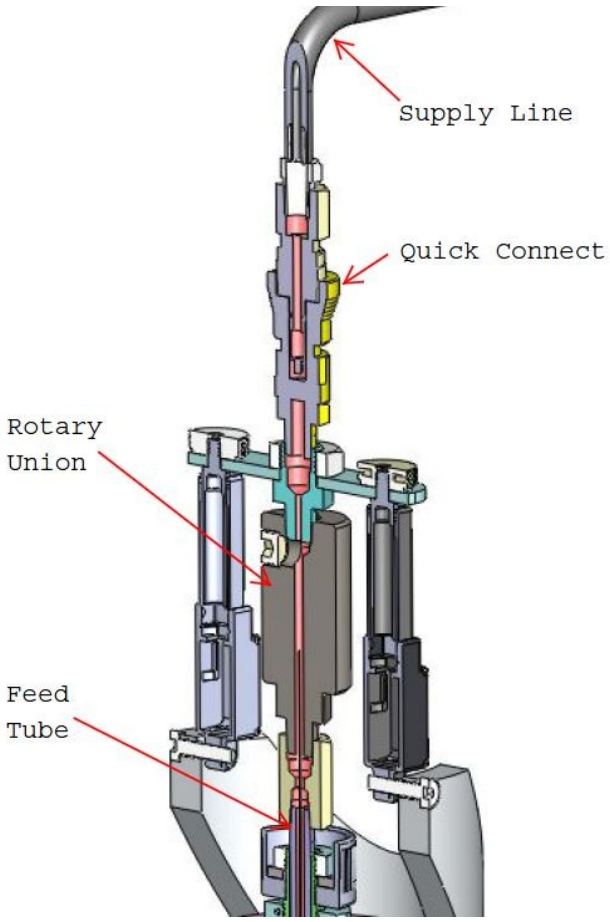

Figure 3.3: Cross section of dielectric fluid entrance

and an exit for the feedback voltage from the spindle, ensuring that the gripper is in contact with the electrode. Much like the fluid path the electrical path must provide a dynamic connection into the spindle. This is performed by using the SR-002 slip ring made by Rotary Systems and is capable of a rotational speed up to 1000 rpm. The SR-002 slip ring utilizes silver graphite brushes running along silver rings to transmit the current into the spindle. The ring allows the use of four separate channels to be connected to the rotating spindle shaft. Three of the channels are used to provide current to the discharging electrode while the fourth is used for the feedback depicted in Figure 3.4.

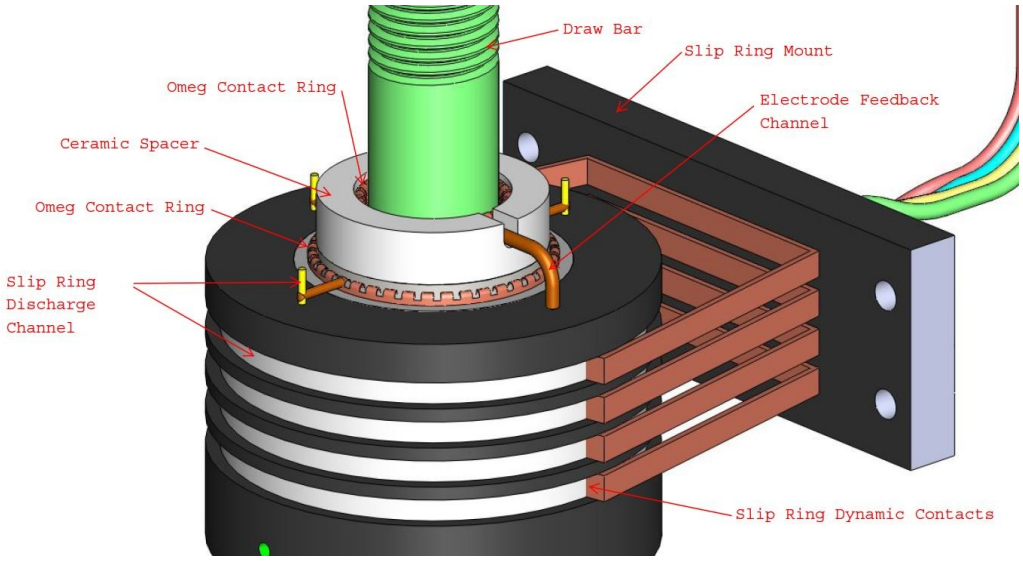

Figure 3.4: Slip ring SR002

The feedback signal that is used to detect the electrode also requires electrical isolation from the rest of the spindle. The feedback path starts between the microgripper and the electrode. The path is continued up the feed tube and into the draw bar. The guides used between the feed tube and draw are conductive D rings made by Parker that facilitate in guiding the feed tube within the draw bar and making a good electrical connection. The draw bar is isolated from the collet using a ceramic draw insert. The draw bar is isolated from the closer by making the preload thrust nut from ceramic. The draw bar is isolated from the spindle by the use of Acetal guides. The feed tube is isolated from the rotary union by the ceramic union coupling. The feedback path leaves the draw bar using an Omeg contact ring to connect the draw bar and slip ring. Figure 3.5 provides insight into how the spindle components are used to provide electrical isolation or conductivity in order to complete the discharge and feedback circuits in the upper portion of the spindle. Figure 3.6 depicts the electrical path in the lower portion of the spindle.

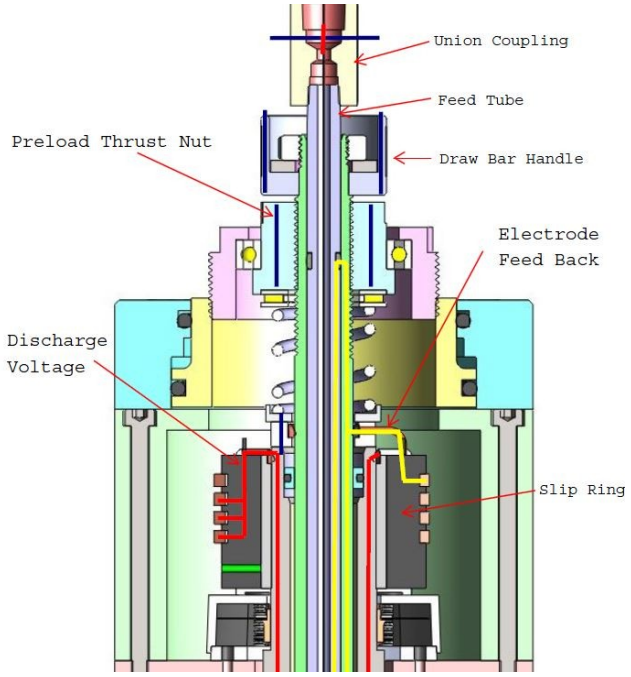

Figure 3.5: Upper electrical path

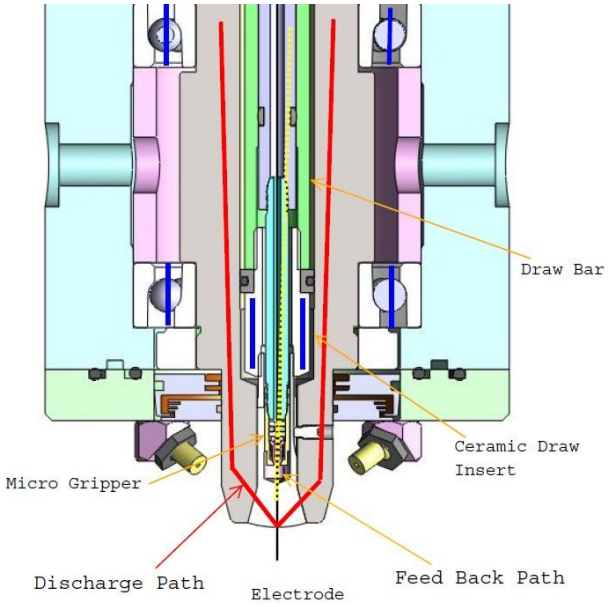

Figure 3.6: Lower electrical path

There are also pneumatic lines that enter into the spindle to actuate the spindle brakes and collet closer. The closer is designed to be used with a three way valve in order to exhaust the pressure from closer's inner chamber. The valve chosen for this design is the Parker EZ Inline Series Air Control Valve. This valve is solenoid operated and is controlled by the machines controller. All the air line fittings are the One Touch series quick connect fittings from SMC. These fittings allow easy assembly without the need to rotate the tube. Figure 3.7 shows how the various pneumatic, hydraulic, and electrical lines plumb into the spindle system.

3.3 1C Closer Design

The closer design is responsible for pulling up on the drawbar to close the 1C collet. The upward force is provided by the Draw Spring. The spring presses down on

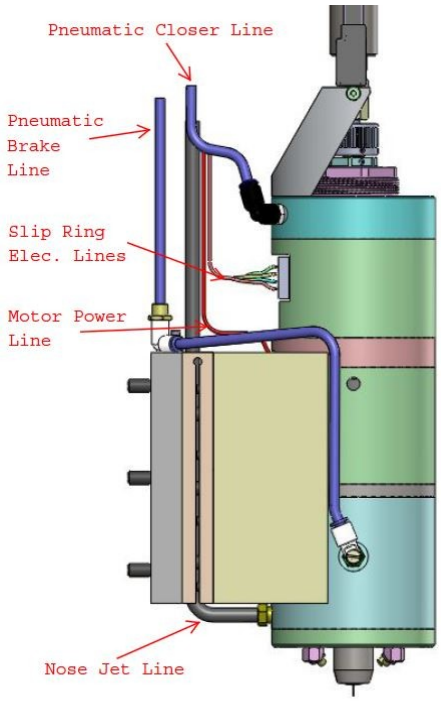

Figure 3.7: External lines

the spindle shaft while pulling the 1C collet up at the nose of the shaft. This configuration cancels the draw, instead of going through the main spindle bearing pack.

The draw force can be adjusted by threading the preload adjust thrust nut down the draw bar. This compresses the draw spring and increases the draw. Using a spring to perform the draw provides the spindle with a passive closing force. No energy is expended to maintain fixturing upon the electrode. Passive closing force is also useful for when the machine is turned off and electrode fixturing needs to be maintained. Figure 3.8 depicts the closer assembly.

In order to open the 1C collet the draw bar needs to be pushed down a short distance. The downward force is provided by the pneumatic pressure chamber and closer collar. The pressure chamber is sealed using o-rings and designed for up to 200 psi.

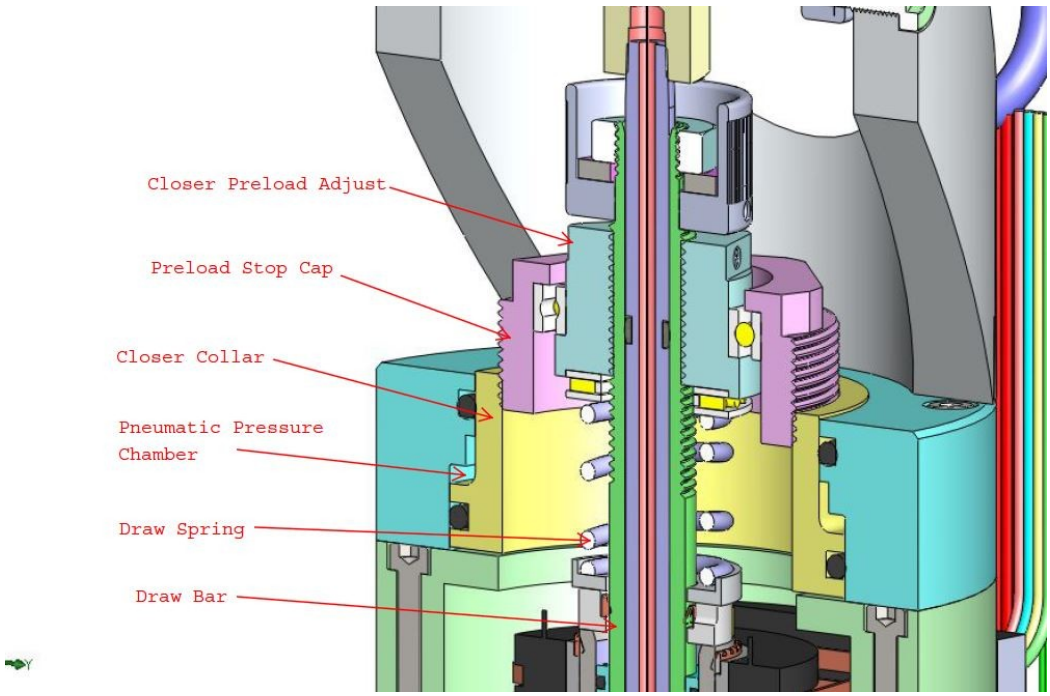

Figure 3.8: Cross section of closer design

When the pressure chamber is charged the closer collar is forced downward through the preload stop cap and thus overcoming the draw spring. The closer assembly includes bearings to address the fact that the preload thrust nut rotates while the closer stop cap and closer collar do not. The bearing is pressed onto the preload thrust nut and given a sliding fit in the bore of the preload stop cap to allow for vertical movement.

When adjusting the draw the preload thrust nut and preload stop cap need to be adjusted together. This is possible because they share the same pitch in their threads. In order to make this process less awkward a tool has been designed for simultaneous adjustment of the two components. Figure 3.9 demonstrates how the tool is intended to be used. Once the desired draw is set the preload thrust nut can be fixed to the drawbar by using soft tipped set screws.

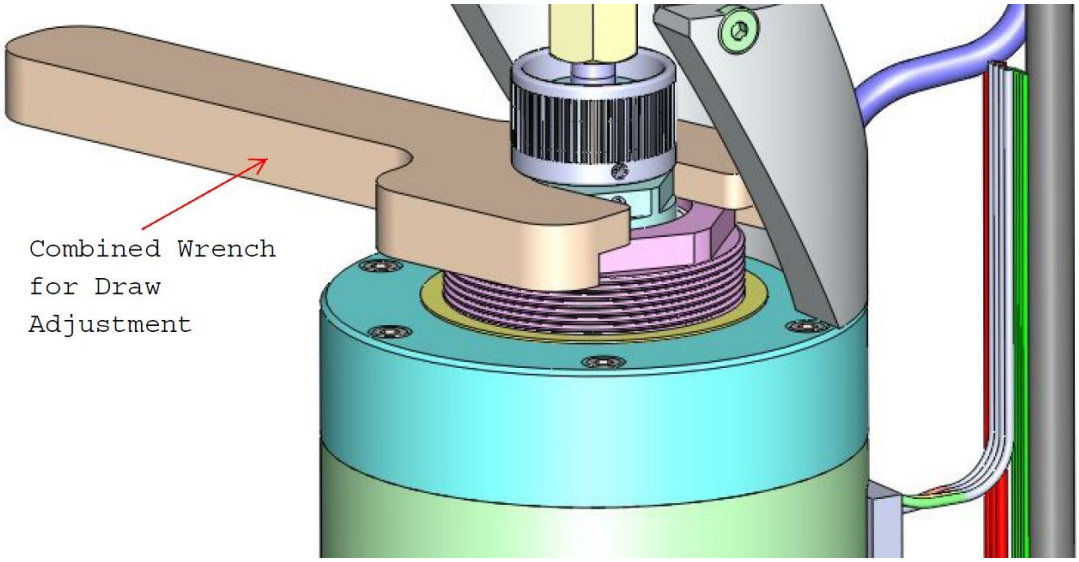

Figure 3.9: Preload adjustment with combined wrench

3.4 Microgripper Design

The hydraulic microgripper is a unique design that uses the preexisting hydraulic system to provide the actuating mechanism to close onto the electrode deep into the center of the spindle. The hydraulic pressure that exists in the feed tube presses the gripper closing collar down onto microgripper collet. As the microgripper is forced down into the closing taper of the gripper collet lid, it is forced to close onto the electrode. When the hydraulic pressure is exhausted, the gripper release spring pushes the microgripper collet out of the closing taper. The closing taper for the microgripper is 30 degrees which is a nonseizing taper allowing the collet to be easily extracted with the 3.4 N of force provided by the gripper release spring. Figure 3.10 depicts the microgripper design. The gripper closing collar houses an o-ring to seal the hydraulic pressure. Under the gripper closing collar is another o-ring which serves as the electrode seal. As the gripper collar is pressed down the electrode seal deformed around the electrode by being forced into the upper taper of microgripper collet. At 1000 psi of dielectric pressure the gripper closing collar presses down on the microgripper collet with 66 N of force. This force is translated into 10 N of gripping force onto the electrode. With the ability to grasp the electrode the feed system with linear actuators can now be used to advance the electrode. The microgripper design is capable of gripping and sealing electrodes from a diameter of 250μm to 1.00 mm, however, the appropriate microgripper collet will need to be installed for the correlating electrode diameter.

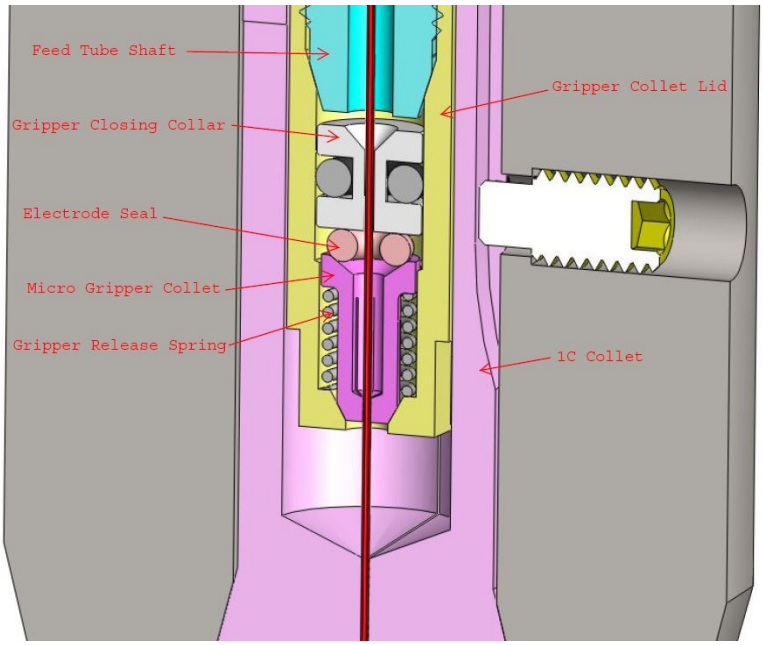

Figure 3.10: Micro gripper design

3.5 Feed System Design

The feed system advances the electrode as the bottom of the tool is worn down. The electrode can be up to 400 mm long when loaded and worn down to 14 mm using the feed system. Electrodes can be worn shorter than 14 mm but the electrode will have to be advanced or loaded by hand. When the electrode is larger than 1mm in diameter then the feed system cannot be used. The feed system design consists of using the 1C collet the microgripper collet and the linear actuators. The 1C collet and the microgripper trade off holding the electrode while the linear actuators feed the electrode down in an inch worm type of motion. Figure 3.11 depicts how the linear actuators advance the feed tube.

The feed sequence begins with the running state configuration, which is both the 1C collet and microgripper collet closed with the feed tube advanced downward. Figure 3.12 shows the running state. Notice the state of the 1C is shown by the I.D. being colored. Red indicates the draw bar is pulling and the collet is closed. Green indicates

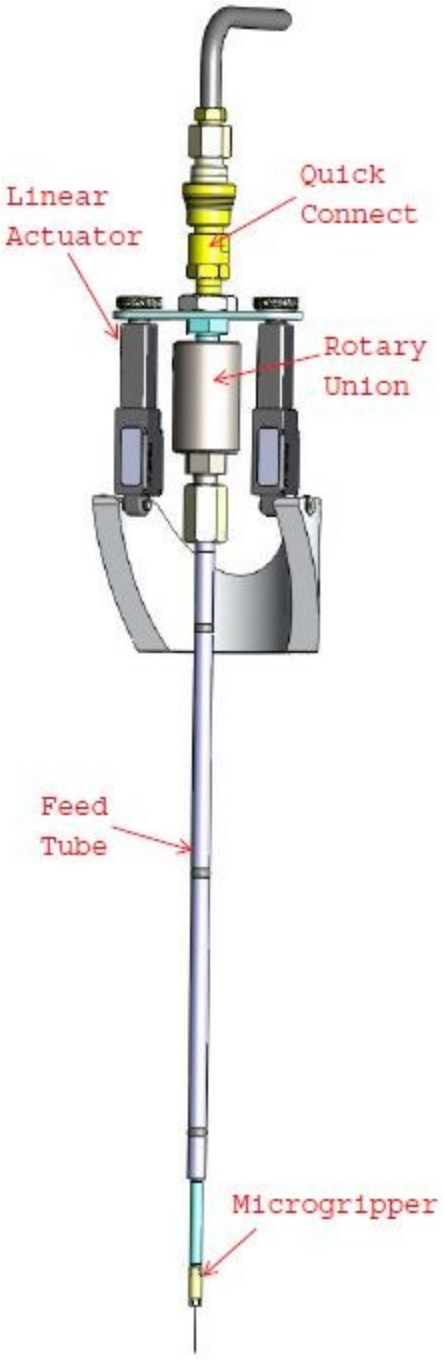

Figure 3.11: Feed system

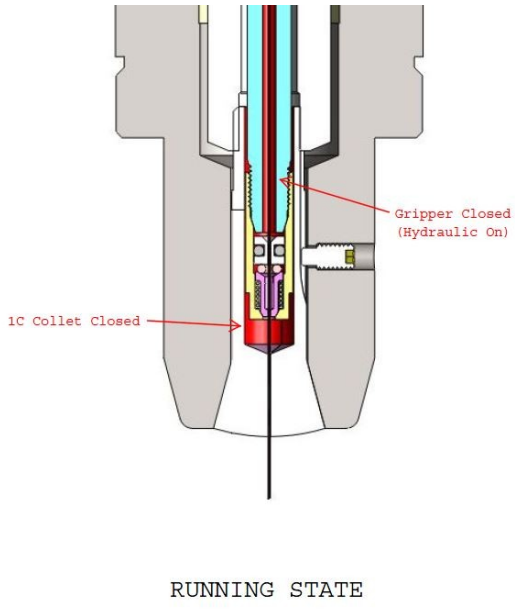

Figure 3.12: Stage 1 of feed sequence

the draw bar is pushing down and the collet is open. The microgripper is also indicated with red in the I.D. of the feed tube being hydraulic pressure on and gripper closed while green indicates no hydraulic pressure and gripper open. The next step of the feed sequence is for the microgripper to release while the 1C collet remains closed. This step of the sequence is depicted in Figure 3.13. Now the feed tube is raised using the linear actuators while the microgripper remains open. This state is depicted in Figure 3.14. The next step is for the microgripper to close and for the 1C to open. This is depicted in Figure 3.15. The microgripper closes before the 1C is allowed to open so that contact with the electrode is never lost. The feed tube is then pushed downward using linear actuators while the microgripper holds onto the electrode. This portion of the feed sequence is depicted in Figure 3.16. To complete the feed sequence the 1C collet is closed and the feed system has returned to its running state.

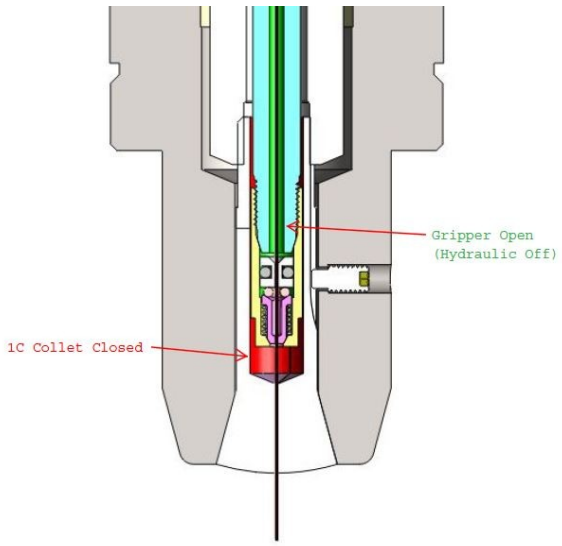

Figure 3.13: Stage 2 of feed sequence

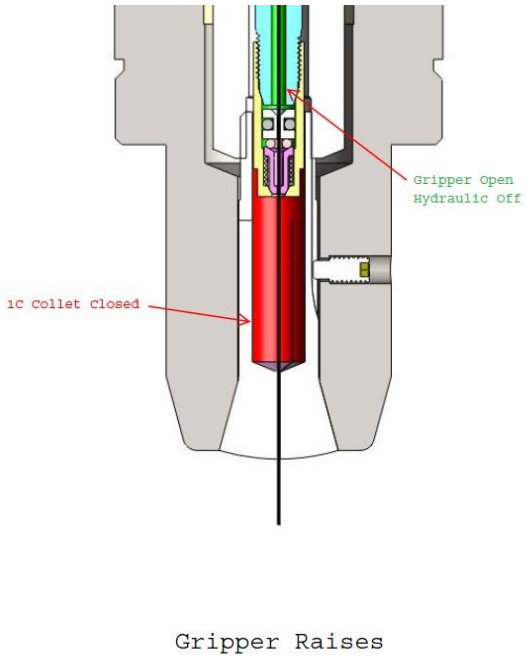

Figure 3.14: Stage 3 of feed sequence

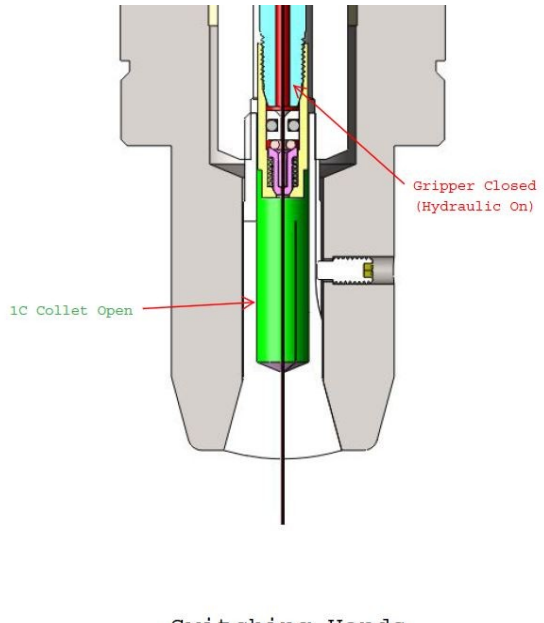

Figure 3.15: Stage 4 of feed sequence

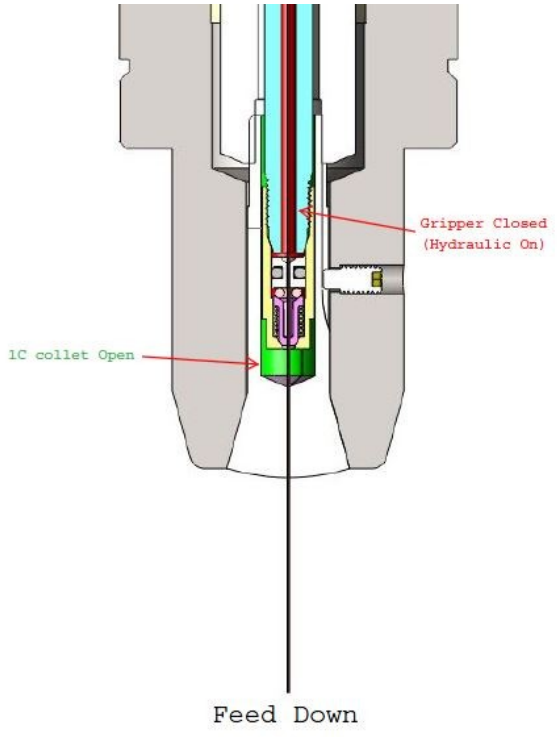

Figure 3.16: Stage 5 of feed sequence

3.6 Spindle Rotation and C-Axis

The spindle design has the ability to provide rotational speed to the electrode along with C-axis positioning. The rotation of the spindle is provided by an electric motor. The motor chosen for the design is one of the Quantum frameless brushless DC servo motors. The QB03401 model was chosen to best match the spindle requirements. This 24V motor is capable of a no load speed of 1722 rpm, a continuous stall torque of 1.57 Nm, and a peak torque of 10.8 Nm. The servo motor is well suited for rotational positioning due to low cogging torque of less than 0.035 Nm. The frameless design allows for the motor to be coupled directly to the spindle shaft and on the spindle's axis. This design is compact and eliminates the need for a coupling device or drive line to the spindle. Figure 3.17 depicts the Quantum frameless motors.

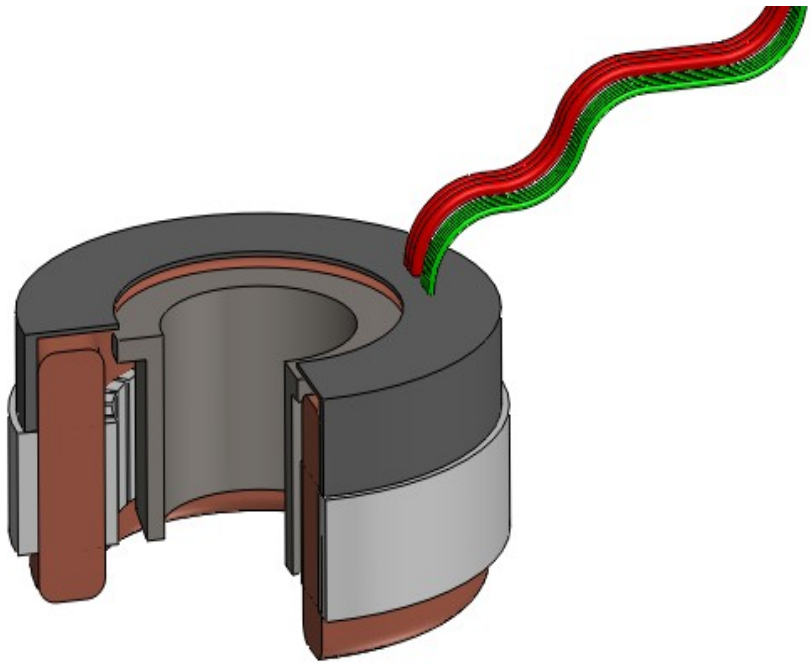

Figure 3.17: Quantum frameless motors

In order to provide accurate positional feedback of the spindle an optical rotary encoder has been incorporated into the spindle design. The encoder chosen is the ENC-A3I high resolution encoder from Anaheim Automation. This encoder was chosen as an economical and compact solution for positional feedback. The encoder like the motor mounts directly to the spindle shaft and in line with spindle's axis with no need for additional couplers. The encoder provides a dual channel quadrature output and is available with 2500 counts per revolution. The encoder also utilizes an index channel for a reference position. The ENC-A3I is depicted in Figure 3.18.

The encoder is used in a closed loop with the motor to provide accurate positioning. The rotational positioning of the electrode is used to produce polygon shaped tools. These types of tools can be produced in conjunction with the WEDG unit and then used to sink various features with sharp internal corners, such as hex or square pockets. Figure 3.19 depicts how the motor and encoder are incorporated into the spindle design.

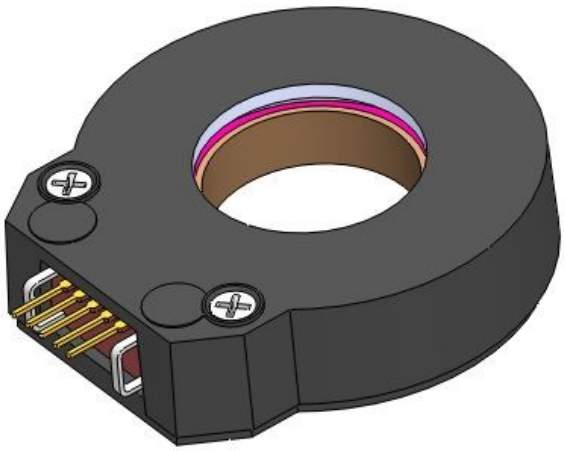

Figure 3.18: ENC-A3I rotary encoder

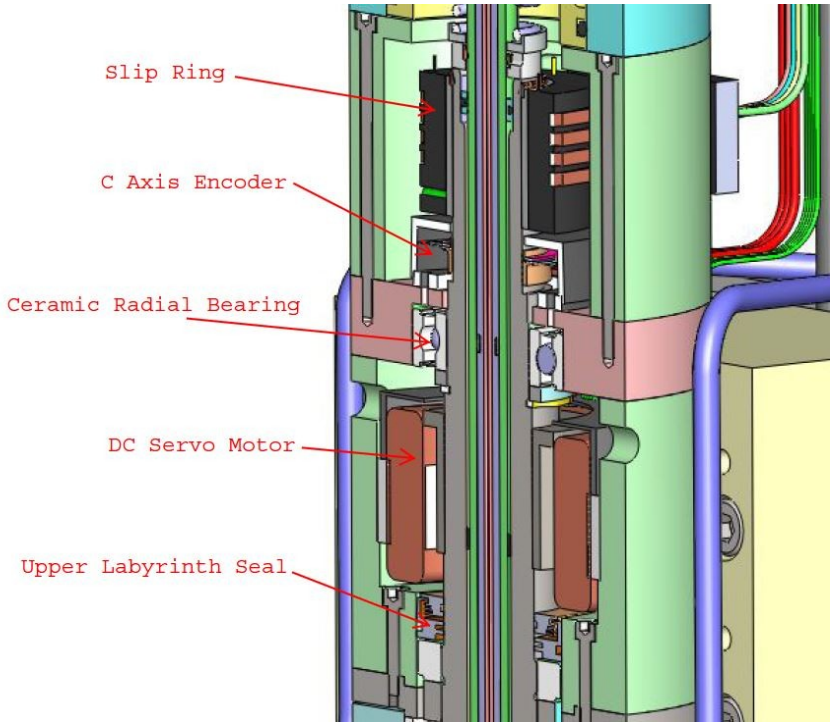

Figure 3.19: Cross section of motor and encoder

In order to provide more accurate long-term rotational positioning of the spindle a pneumatic brake system was designed into the spindle housing. Some amount of positional error is encountered as the spindle rotates between the encoder poles. When attempting to hold a position without the use of a brake the motor must maintain the position by watching for change in the pole position of the encoder. This allows for dithering of the spindle between the encoder poles and leads to increased heat generation from the motor. Dithering of the spindle affects how flat and accurately the cut features will be when using the WEDG unit and sinking the electrode. The heat generated from the motor will also affect the accuracy of the spindle as the heat causes deformation of the spindle and induces a change in the spindle bearing preload. The brakes eliminate the servo dithering and allows the motor to shut off once the desired position has been

obtained. Figure 3.20 demonstrates how the brake contacts the spindle and how the brake is incorporated into the design. Since the EDM process is relatively slow, it is expected that the spindle will be required to frequently hold a fixed angular position for long periods of time. This aspect of the spindle's function makes the addition of a brake more critical and leads to more accurate and efficient cutting. The brakes are easily accessible for service and replacement and are an economical solution for braking the spindle.

3.7 Seals and Guides

The spindle design requires different types of seals and guides to help perform virtually every function of the spindle. O-ring seal designs are used for pneumatic and hydraulic sealing. O-rings are also used in the polytetraflouroethylene (PTFE) guides to help guide and secure the draw bar within the spindle shaft. The feed tube uses

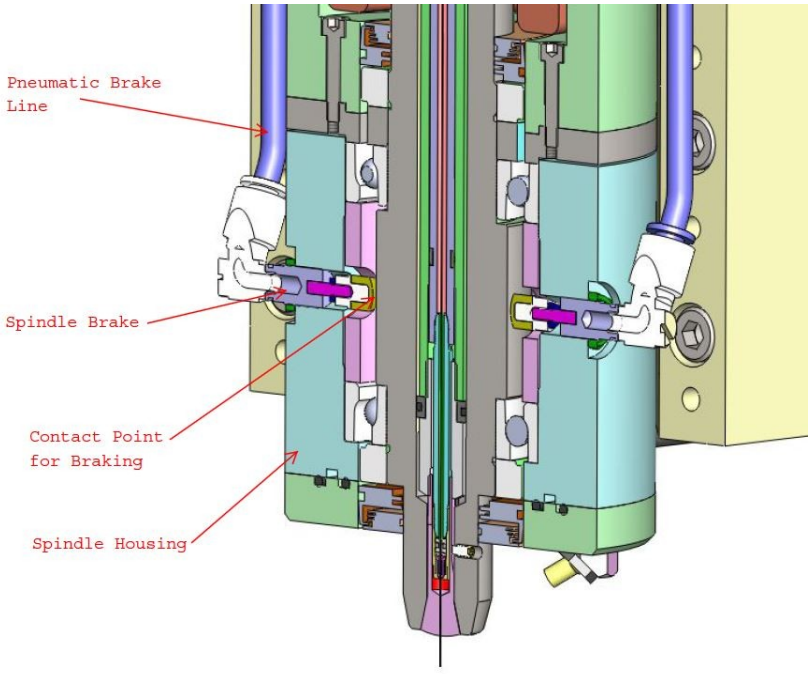

Figure 3.20: Pneumatic brake design

conductive D-rings to help make electrical contact and to help guide the feed tube in the draw bar. The spindle bearings require seals to facilitate in keeping foreign material out of the races. The spindle design incorporates noncontact labyrinth seals to perform this task with no rotational drag.

O-rings are the most extensively used seals in the spindle and have been designed at each location with specific fits to perform sealing. In order to determine the appropriate fit for each o-ring seal the Parker O-Ring Handbook was used [25].

The pneumatic closer requires sealing of air at 120 psi. For the closer design a floating pneumatic ring seal gland was used. Figure 3.21 depicts the use of this seal gland in the closer design. In this seal design the piston gland incorporates an o-ring that

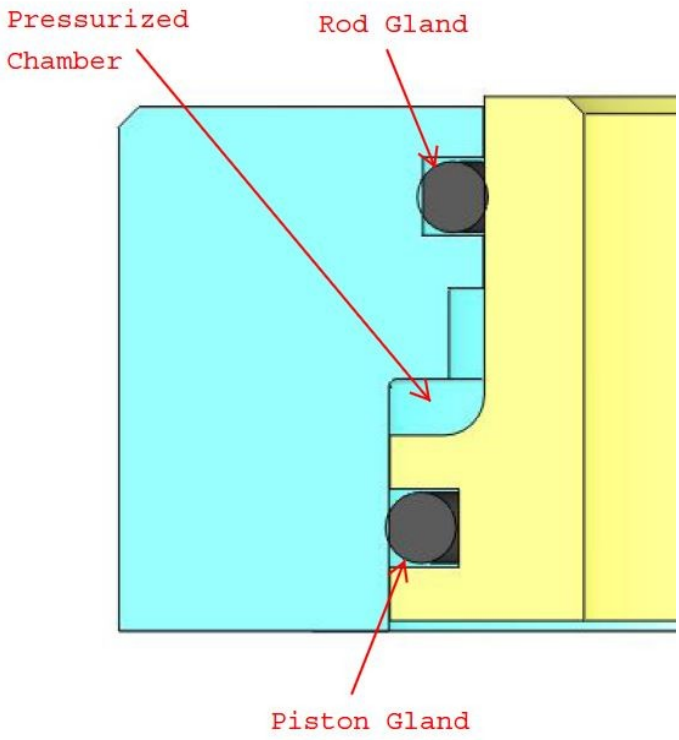

Figure 3.21: Closer o-ring design

has virtually no squeeze. Figure 3.22 demonstrates the o-ring fit of the floating lower o-ring in the piston gland. The looser fit in this type of seal allows for a 60% reduction in the break out friction for the closing collar [25]. The rod gland is a standard industrial reciprocating o-ring gland.

The hydraulic lines for the high pressure nose jets are able to seal up to 1000 psi of deionized water. This seal design is a face seal type and uses two o-rings to seal both sides of the nose jet channel. Figure 3.23 depicts the face seals and the design of the nose jet channel. The face seal is a static design which utilizes a high squeeze of 30% and is capable of sealing high pressures [25].

O-rings are also used in the draw bar guides. These o-rings do not perform any sealing but rather help secure and guide the draw bar. Since these o-rings are compressed 10% they create running friction when the draw bar is moved. Using the Parker O-Ring Handbook the running friction produced by these o-rings is approximated at 12.3 N. Figure 3.24 depicts the use of these o-rings in the draw bar guide. In order to provide a smooth surface for the guides to run on the bore of the spindle is reamed.

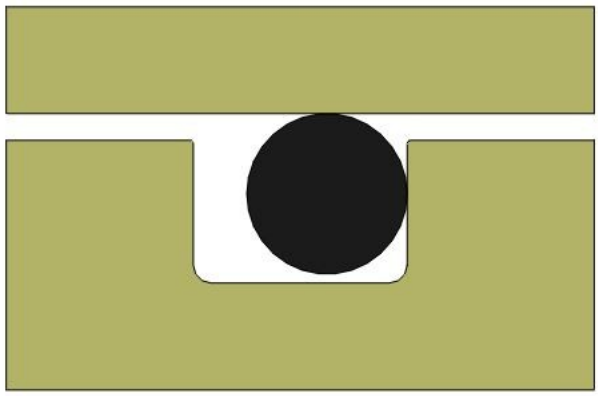

Figure 3.22: Floating o-ring design [Adapted from 25]

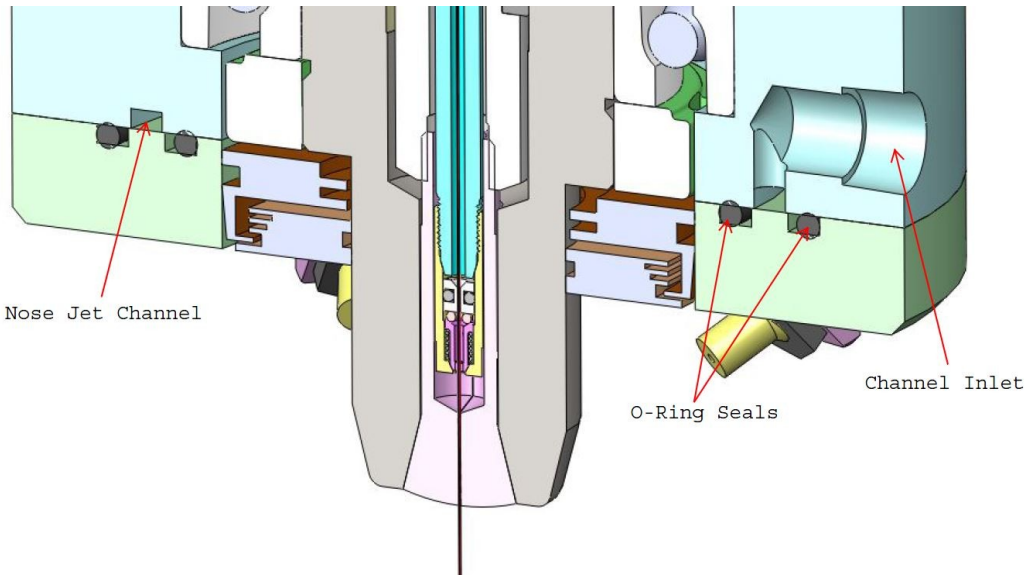

Figure 3.23: Nose seal design

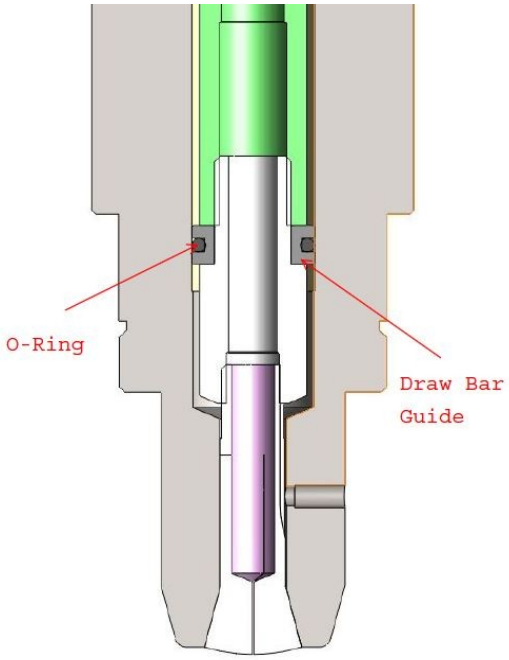

Figure 3.24: Draw bar guide design

3.8 Bearing Pack Design

At the heart of the mechanical design is the spindle bearing pack. The bearing configuration is responsible for low run out of the electrode and the overall stiffness of the assembly. Since low run out of the spindle is of critical importance the bearings must be chosen carefully. Angular contact bearings were chosen for the spindle due to their high accuracy and rigidity. Angular contact bearings are available in a large variety of sizes offering a compact bearing option. Angular contact bearings are designed to be loaded in only one direction and for this reason the bearings are arranged in pairs. The bearings are typically arranged so they oppose one another allowing loads to be applied in either direction. When two bearings are used they can be arranged face to face, back to back, or in tandem. Arranging the bearings in tandem provides higher strength and rigidity in one direction but the arrangement cannot take any load in the other direction, and another bearing opposing the tandem pair needs to be added. Figure 3.25 depicts the differences between these orientations.

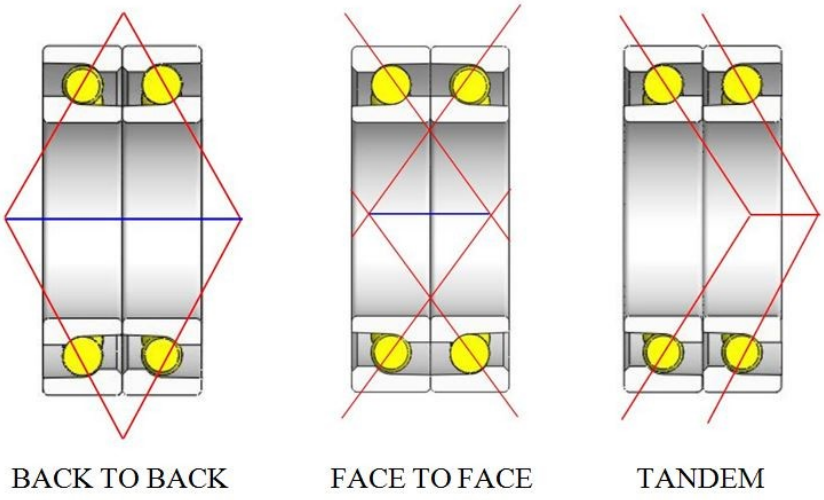

Figure 3.25: Angular contact bearing orientations [Adapted from 26]

In order to allow loads in both directions and only use two bearings the back to back or face to face arrangement needs to be chosen. The back to back arrangement provides more rigidity due to the direction of the load lines. The distance between where the load lines cross the axis of rotation provides bending stiffness to the spindle and is known as the effective bearing length [27]. This can be seen in Figure 3.26. An increase in the effective length increases the spindle stiffness. Figure 3.27 depicts this relationship. This increase in effective length can be achieved by mounting the bearings further apart and by increasing the contact angle of the bearing. The face to face arrangement reduces the effective length and spindle stiffness. If low spindle rigidity is required such as in the case of self aligning spindles then the face to face arrangement is commonly applied.

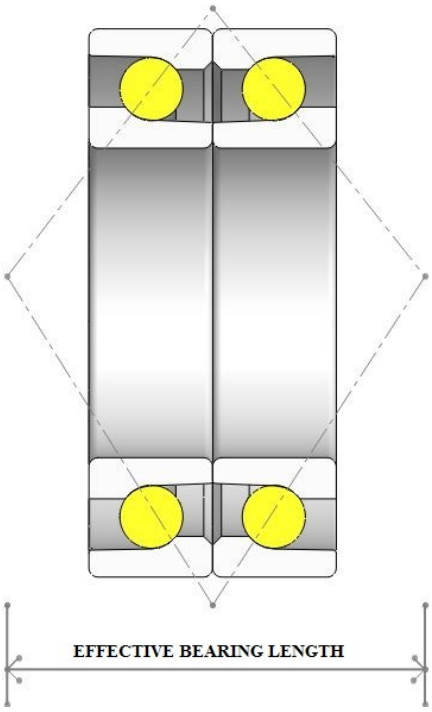

Figure 3.26: Back-to-back effective bearing width [Adapted from 27]

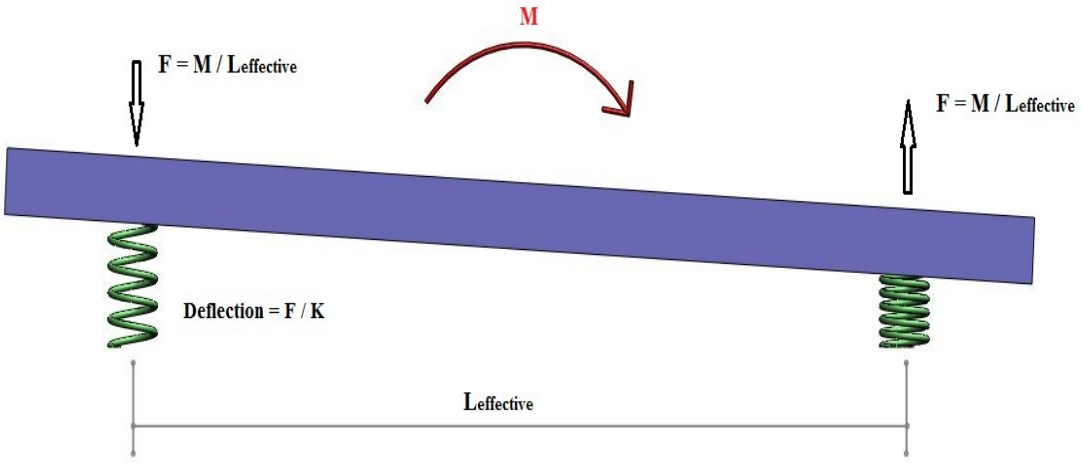

Figure 3.27: Effect of bearing spacing [Adapted from 27]

Spindle rigidity can also be increased by applying a preload to the pair of angular contact bearings. This preload is achieved by pressing the inner race into the bearing and thus taking up the clearance between the inner race, the rolling elements, and the outer race. The preload needs to be set at the desired amount since too much preload will cause premature failure and too little preload will cause a loss of accuracy and rigidity.

Another consideration in the bearing arrangement is how thermal expansion of the spindle shaft will affect the preload. When using the face to face arrangement the preload is increased as thermal expansion occurs. As the spindle shaft lengthens up its axial direction the bearing preload increases as the inner races grow further apart. As the spindle shaft expands in the radial direction the inner race also expands in the radial direction causing further increase in the preload. The back to back arrangement shows much more favorable behavior during thermal expansion of the spindle shaft. The back to back arrangement is known as being "thermocentric," as the expansion of the inner races in the axial direction decreases the preload while thermal expansion of the inner

races in the radial direction increases the preload [27]. The two expansions to some degree cancel one another allowing the preload to remain less affected by thermal growth.

In the EDM spindle the accuracy is the primary goal of the bearing arrangement. Optimal accuracy is achieved by designing the components to be manufactured in such a way that the when the components are machined re-chucking is not required. The materials the components are made from are also an important factor in the accuracies achievable when machining the bearing seats.

Since deflection of the spindle causes errors in accuracy the rigidity becomes an important spindle characteristic. The spindle does not see tool loads, which reduces rigidity requirements to minimizing the deflection of the spindle due to its rotation. Spindle rigidity minimizes the effects of vibration at increased rotational speeds. In the current spindle design the anticipated spindle speed of 1000 rpm is relatively low but the spindle shaft is slender with an aspect ratio of greater than 10. This slenderness makes the spindle shaft susceptible to whipping, requiring more spindle rigidity to minimize electrode run out.

Since EDM machining takes a long period of time it is expected that the spindle motor will run continuously for periods in excess of 24 hours. This long run time means that the motor will produce a significant amount of heat causing thermal expansion in the spindle.

The EDM spindle design employs a bearing arrangement that is suited to the needs of an EDM spindle. In order to achieve greater spindle rigidity and a spindle less susceptible to thermal fluctuations the back to back arrangement of two angular contact

bearings was used. Figure 3.28 shows the design of the back to back arrangement in the lower section of the spindle. The spindle shaft, spindle housing and bearing spacer are made from 17-4 precipitation hardened stainless steel. These three components are made from the same material to minimize the effects of thermal growth as the materials will grow at the same rate. The 17-4 stainless was chosen for several reasons. This material has a similar thermal expansion rate to that of the alloy steel races of the bearings. The 17-4 stainless can be easily hardened and has relatively good stability due to low amounts of stress relieving. The 17-4 stainless is easily machined and is a magnetic material allowing the use of a magnetic chuck used in surface grinding. The 17-4 stainless is resistant to oxidation and does not require additional surface treatment that degrades the tolerances of the components.

In order to increase spindle rigidity the angular contact bearings have been separated 42 mm by the use of the bearing spacer. The lower angular contact bearing is secured to spindle shaft by the use of a lock nut that it is set and then secured using a set screw. The lock nuts used are the KMK series precision lock nuts from SKF. The lower angular contact bearing is then secured downward into the spindle housing through the bear spacer. The upper angular contact bearing is secured by the outer race being pressed downward into the bearing spacer by the upper bearing cap. The upper bearing cap also made from 17-4 is precision ground where the cap contacts the bearing. The upper bearing cap is secured using six M4 socket head cap screws. Figure 3.29 demonstrates how the lower bearing pair incorporates into the spindle assembly. Figure 3.29 also demonstrates the use of the noncontact labyrinth seals which are used to keep the bearings clean. The seals chosen are from the Parker LN series. The LN series is

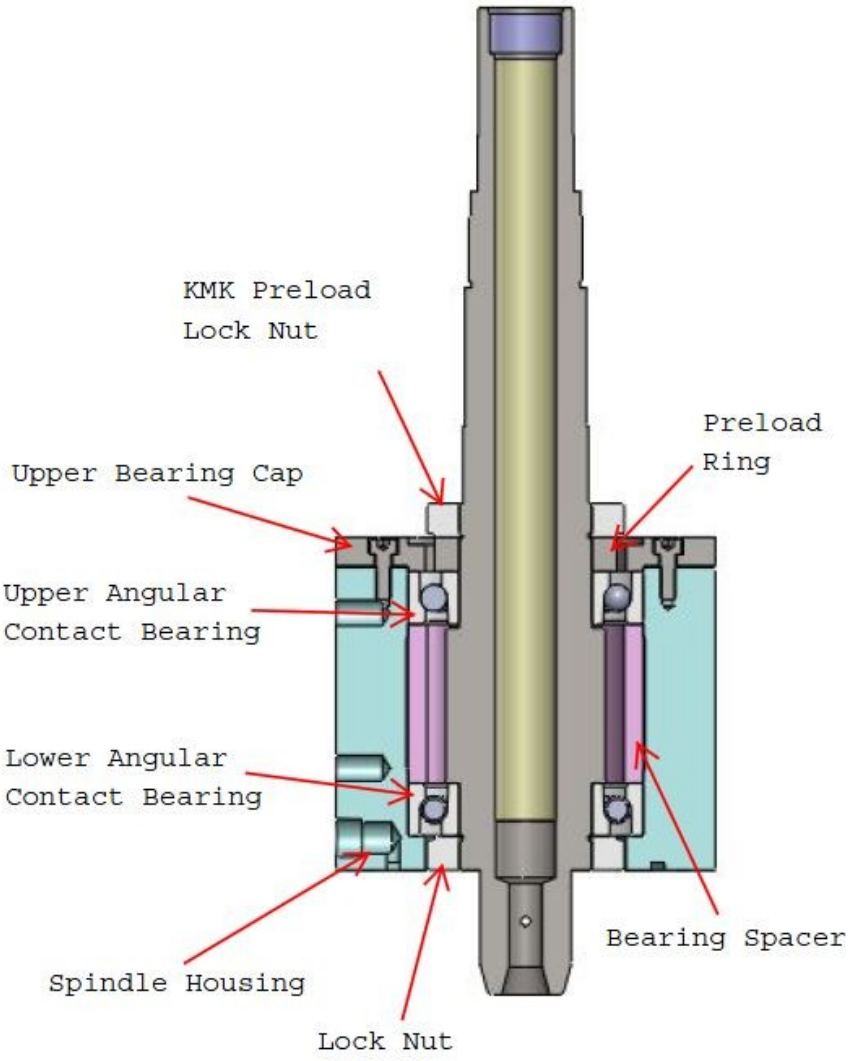

Figure 3.28: Spindle bearing back-to-back configuration

of a vertical orientation and is effective at sealing heavy water spray and dust. The LN series can also be run dry as there is no contact.

The preload is applied by the use of the upper KMK precision lock nut. The upper lock nut is torqued down with a spanner wrench from SKF. When torque, the lock nut presses down on the preload ring, which presses down on the inner race of the upper angular contact bearing. As the inner race is pressed down into the outer race the

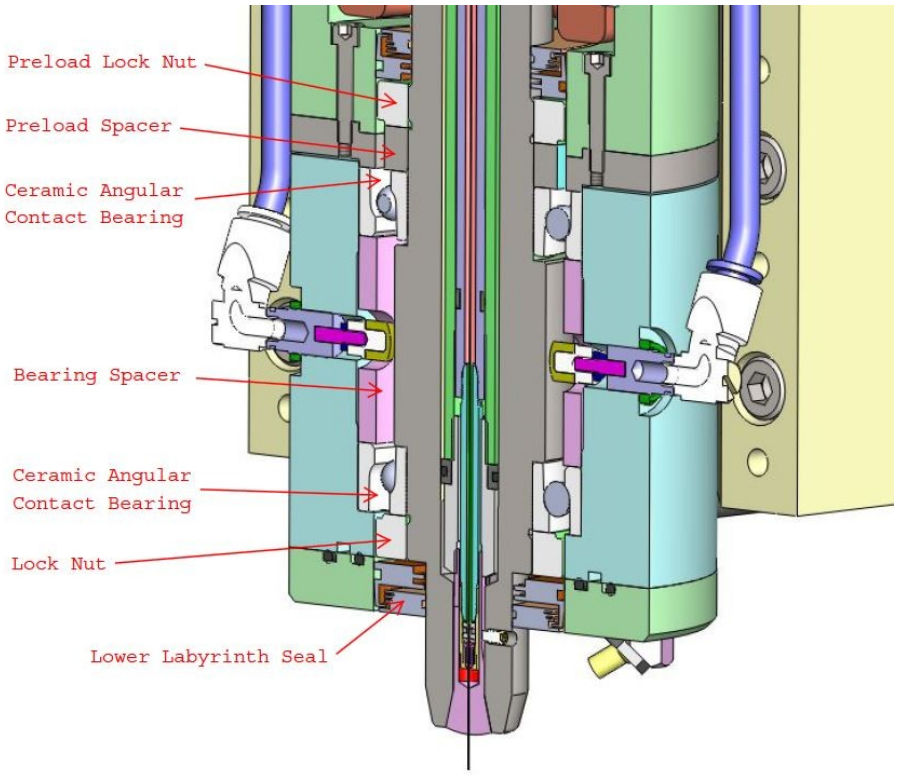

Figure 3.29: Lower spindle cross section

bearing clearance is taken out. As torque is applied to the upper lock nut the spindle shaft is drawn upward into the housing. As the spindle shaft is drawn upward the inner race of the lower angular contact bearing is drawn up into the outer race. The upper and lower angular contact bearings are now preloaded against each other. Figure 3.30 demonstrates how the preload is applied. Figure 3.30 also shows the positions where clearance is designed to ensure that the components contact the bearings in the correct locations. There is clearance under the upper bearing cap between the cap and the spindle housing. This ensures the correct fixing force on the outer race of the upper angular contact bearing by only contacting the outer race. Clearance is also designed under the inner race of the upper angular contact bearing. This clearance is provided so that the inner race can

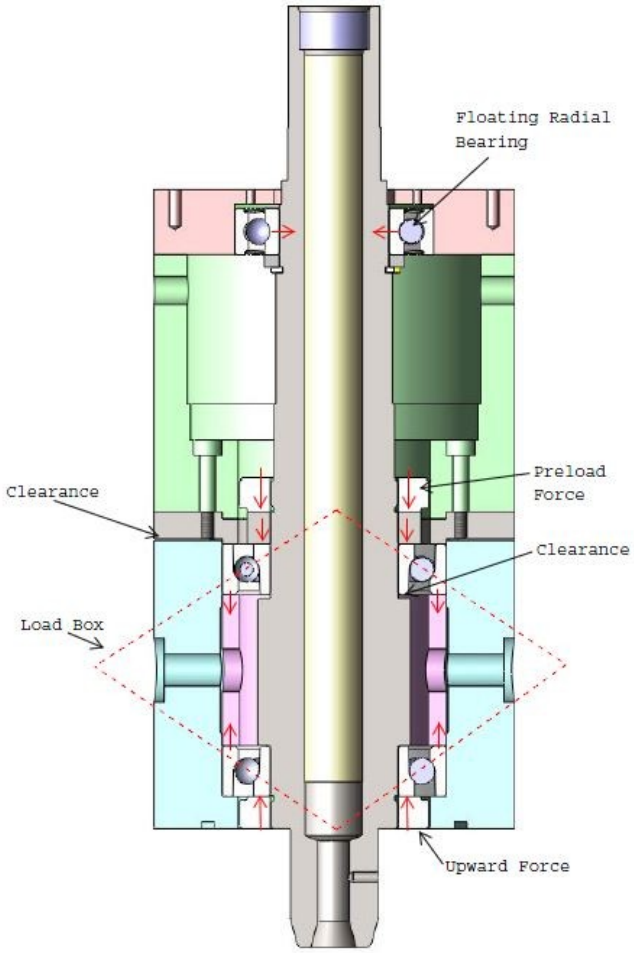

Figure 3.30: Bearing preload design

move relative to the spindle allowing for the bearing to be preloaded. This clearance also ensures all the preload force runs through the bearing elements and into the outer race. Figure 3.30 also demonstrates the deep groove ball bearing used in the upper portion of the spindle shaft. This bearing is designed to capture the upper end of the spindle and reduce any whipping of the spindle shaft while rotating. This bearing is intended to apply radial support only. The bearing is allowed to float in the axial direction to allow thermal expansion of the long spindle shaft. The deep groove ball bearing is pressed onto the

spindle shaft and axially located by using a snap ring and abutment collar. The outer race of the bearing is given a locational clearance fit with the bore of the motor housing lid. This fit provides accurate location of the bearing while still allowing motion with a light force [28]. Clearance is provided above the bearing to allow movement of the outer race during thermal expansion.

The placement of the bearings is of great importance due to its influence on the spindle's rigidity. In order to achieve optimal spacing of the bearings on the spindle shaft the deflection curve for the shaft was determined with the bearings at a given location. This study can be seen in Chapter 6. This study also includes estimations of each bearing's axial and radial stiffness.

The spindle bearings do not only serve as rotational guides but as electrical insulators to insulate the discharge voltage between the spindle shaft and the spindle housing. Primarily for this reason hybrid SKF precision angular contact bearings were chosen. The SKF 7007CE/HC PA9A is the angular contact bearing chosen. This hybrid bearing meets ABEC 9 standards and has a contact angle of 15 degrees. These hybrid bearings have an alloy steel outer race and inner race while the rolling elements are silicon nitride. The silicon nitride rolling elements provide several advantages to the spindle assembly. The silicon nitride balls effectively insulate the encountered voltages by providing a specific electrical resistance of 10^{18} ohm·mm^2/m to the precision hybrid bearings. The ceramic balls also provide more radial and axial stiffness as the silicon nitride balls have up to a 50% higher modulus of elasticity than standard steel balls [29]. The silicon nitride also produces less friction in the bearing than the steel balls. This reduction in friction turns into less power loss, less heat generation, quieter running, and

a dramatic increase in service life. Figure 3.31 graphically demonstrates the advantages of silicon nitride elements associated with service life, radial stiffness and axial stiffness. The silicon nitride balls have a lower density than steel balls allowing the hybrid bearings to have lower centripetal forces and higher accelerations.

3.9 Spindle Fixturing and Alignment

The EDM spindle is designed to be fixtured into a machine platform through an alignment assembly. The alignment assembly consists of the V-block, the YZ adjust, and the base plate. Figure 3.32 shows the spindle mounted to the alignment assembly. The motor housing and spindle housing are secured to a precision V-block. The V-block is positioned by the YZ adjust flexure to align the pitch of the spindle in the machine platform. The YZ adjust is designed to provide 2.3 mm of deflection at the end with only 170 N of force. Figure 3.33 demonstrates the deflection of the YZ adjust at 170 N. The YZ adjust is pulled down and fixtured by the mounting bolts for the V-block and adjusted

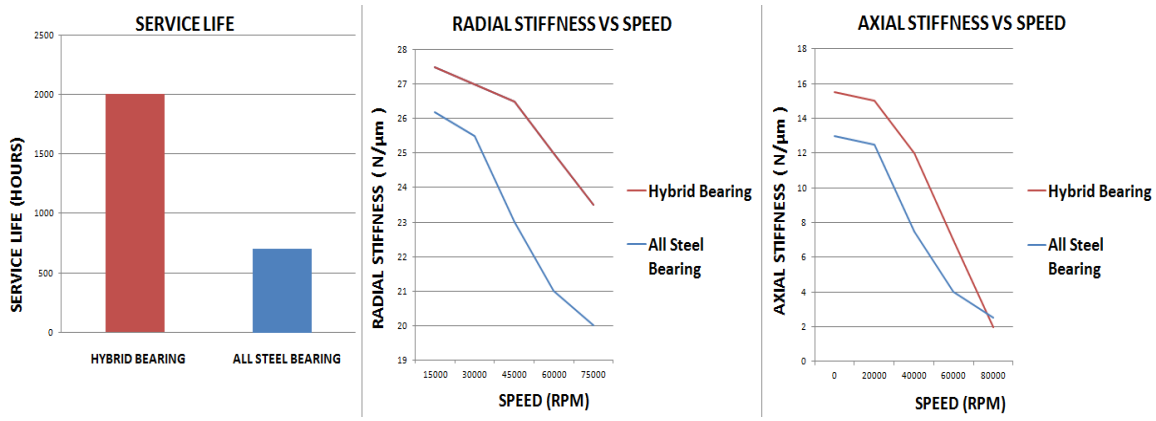

Figure 3.31: Advantages of hybrid bearings [Adapted from 29]

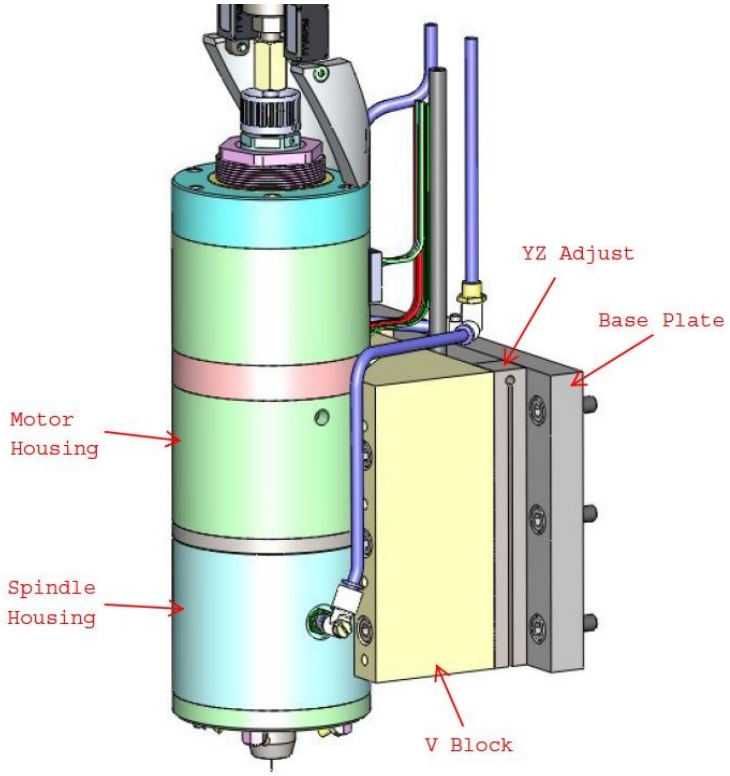

Figure 3.32: Spindle fixturing

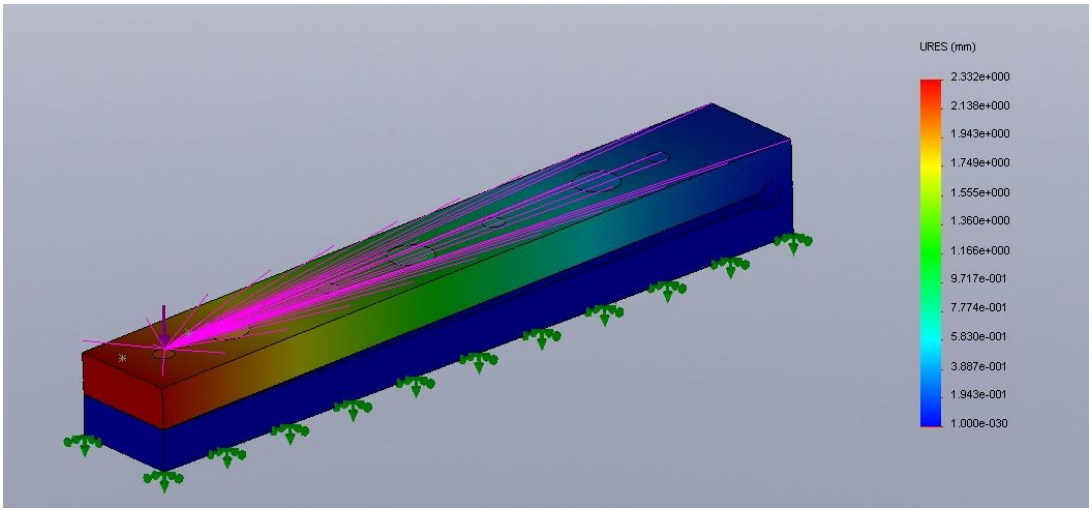

Figure 3.33: Deflection of YZ Adjust

up or down with three M5 set screws that are accessed through the V-block. The spindle is adjusted for yaw in the machine platform by the use of a precision pin that is pressed into the back of the base plate. The pin is used for easy rotation of the base plate and simplifies dialing the spindle axis into alignment with the machine axis.

3.10 Machine Setup

The EDM spindle was designed to be part of a machine platform. It is through this platform that all of the features of the spindle can be integrated. The machine setup consists of three linear axes, a WEDG unit, a deep hole guide, a hydraulic system, a pneumatic system, a tank and a granite structure. The completed machine setup would require a more refined design including a control system, an enclosure, and routing of the hoses and cables. Figure 3.34 gives a depiction of what a machine setup might look like.

The tank design is an economical and simple method for being able to perform submerged flushing. The tank walls are made from acrylic and are joined together using acrylic glue that seals the joints extremely well. The tank is really only a simple addition to the base plate that is needed regardless of the tank. The tank is clamped down to the base plate with corner braces over the tank and long bolts that thread into the base plate. In order to seal between the base plate and the acrylic tank an o-ring is used. The o-ring sits in a groove machined into the base plate and is deformed as the tank is pulled down. Figure 3.35 shows a similar tank that includes an overflow so that dielectric fluid can be continuously cycled through the tank.

The base of the tank is designed for fixturing precision components and workpieces into the machine. The base plate is precision ground and offers an array of threaded holes for fixturing.

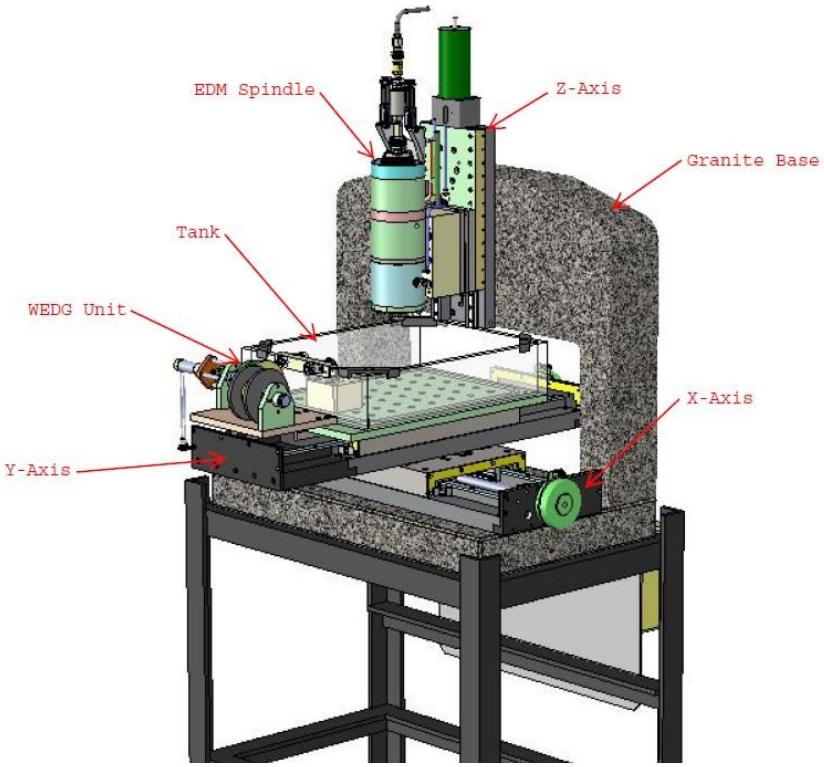

Figure 3.34: Machine setup

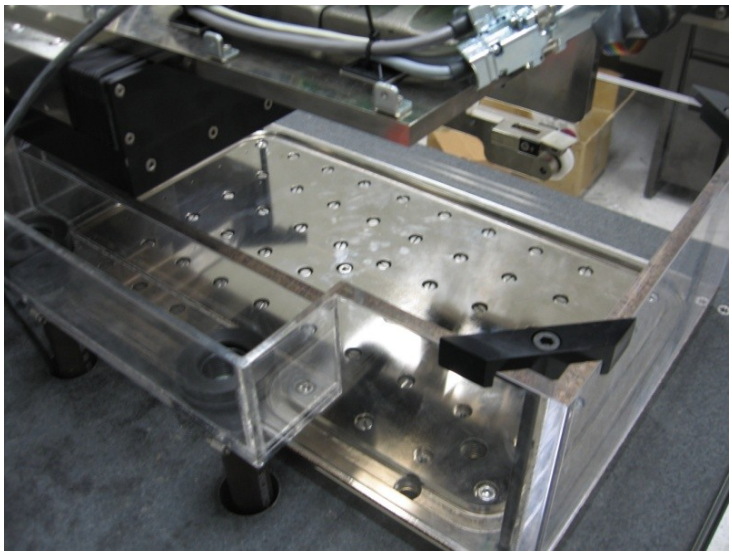

Figure 3.35: Tank design

The linear axes are an important aspect of the machine platform as the axes are responsible for the positional accuracy of the machine. The X and Y axes position the workpiece while the Z-axis positions the electrode. The axes are designed to provide accuracy and smooth running motion. These axes utilize smooth running crossed roller guides for the linear bearings. In addition to being smooth running the crossed roller guides provide accurate and rigid motion. The downside to this type of linear bearing is its limited travel however for the micro EDM platform the needed travel is easily obtained. Figure 3.36 shows how the guides are configured into a linear axis. The position of the axis is determined using linear encoders. Linear encoders provide an accurate location of the axis and do not suffer from inaccuracies associated with any backlash in the drive system. The drive of the axis is provided by a DC motor and a ball

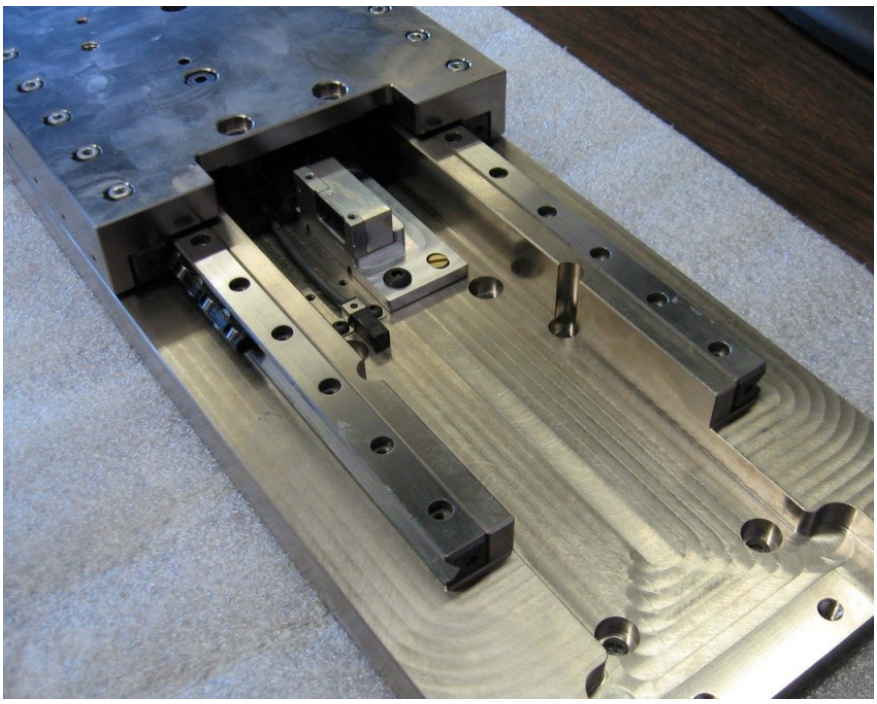

Figure 3.36: Crossed roller guides

screw. The ball screw has a preloaded nut to eliminate backlash and utilizes angular contact bearings in the support unit to accommodate for the thrust.

The X and Y axes are capable of an accuracy of 1µm over the travel distance of 250 mm. The Z axis is also capable of accuracy of 1µm and offers 150 mm of travel. Figure 3.37 shows the X and Y axes stacked and perpendicular to one another. Figure 3.38 demonstrates a similar configuration of the Z axis and granite structure.

The axes have been designed so that the components are centered as much as possible. The ball screw runs directly through the center of the linear bearings and the motor mounts directly to the end of the ball screw. The encoder is near the center as well. This design improves the accuracy of the slide and reduces the possibility of backlash in the linear slide. This is an important feature when EDM machining due to

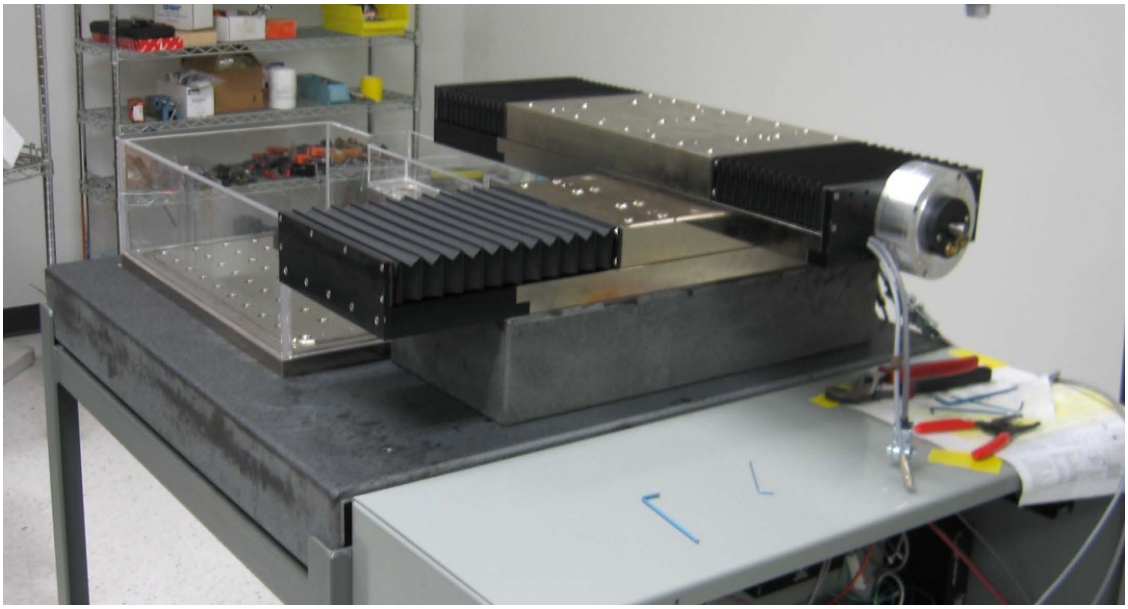

Figure 3.37: Linear axes

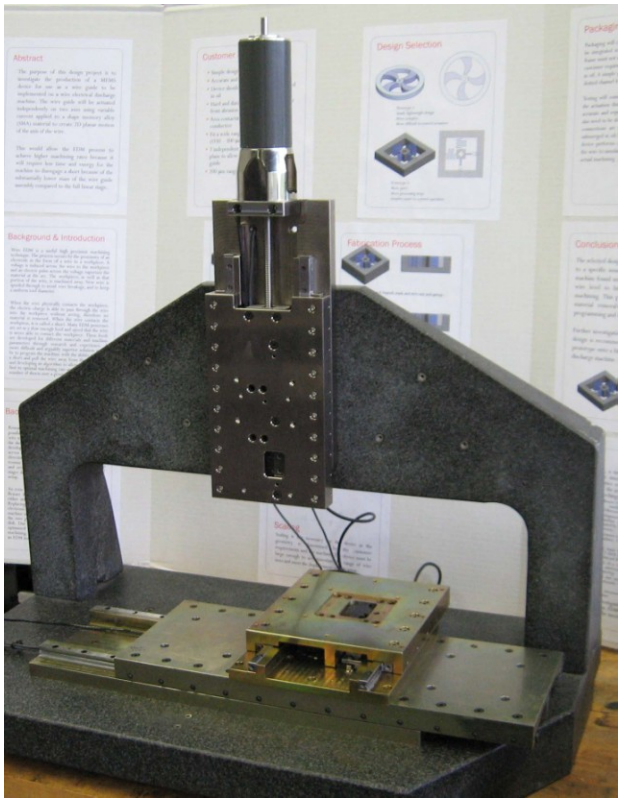

Figure 3.38: Three-axis setup on granite

the rapid and precise movements involved with the servo motion of the electrode when shorting occurs.

The wire dresser or WEDG unit is a critical feature in a machining platform for the EDM spindle. The WEDG unit that was designed for use with the EDM spindle is shown in Figure 3.39. This unit was designed to use standard spool sizes making it easy to load spools of wire that are economical and readily available. The precision wire guides are made from ruby and the contact is made from carbide. The base of the unit is precision ground 17-4 stainless steel. The V-groove pulleys are made from polyacetal and ride on a radial ball bearing. The wire is drawn by being wound up on the drive spool. The drive spool is driven by a DC motor with a built in gearbox.

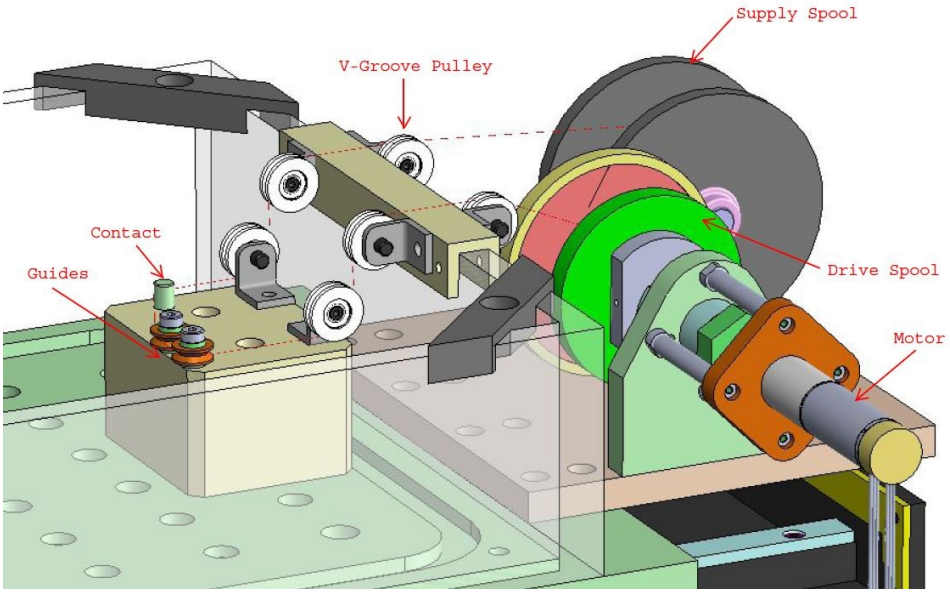

Figure 3.39: Wire dresser design

The WEDG unit allows versatile fabrication of electrodes. The EDM spindle is capable of chucking electrode material in a wide range of sizes up to 6 mm in diameter. The ability to hold small and large electrodes gives the spindle a unique ability to be coupled with a WEDG unit and make a variety of electrode shapes and sizes. Figure 3.40 provides some sample shapes that can be produced using the WEDG unit. The WEDG unit is also a powerful tool in creating electrodes for popping microholes. When using the WEDG method, electrodes as small as 5µm in diameter can be created.

The proposed machine setup also includes a deep hole drilling guide. This guide helps to support long slender electrodes as they are used to plunge into deep holes. The guide design is simple and adjustable. The guide is secured to the stationary portion of the Z-axis and is adjusted manually to the desired height above the workpiece. The guide rails are precision ground for improved accuracy. The tube guide is a Sodick TS guide

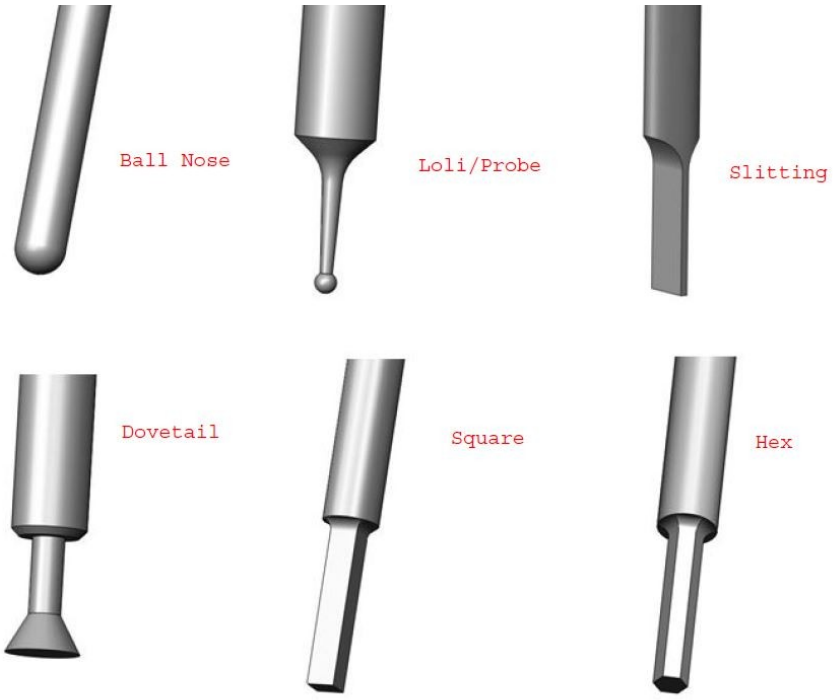

Figure 3.40: Electrode shapes

and it is available in a variety of sizes. The size of the guide needs to be just over the size of the electrode being used. The inner portion of the guide is made from ceramic and insulates the electrode. Figure 3.41 depicts the deep hole drilling guide in the machine platform. The deep hole guide allows long sections of electrode to be exposed without whipping occurring during rotation. The guide supports the electrode just above the workpiece and remains stationary as the Z-axis moves up and down. While using the deep hole guide the Z-axis is used to peck by rapidly moving into and out of the deep hole. This pecking motion assists with the removal of EDM debris and reduces shorting. The machine setup also includes a mockup of the hydraulic system. The Tescom system may be panel mounted or purchased in an enclosure. This mockup demonstrates the

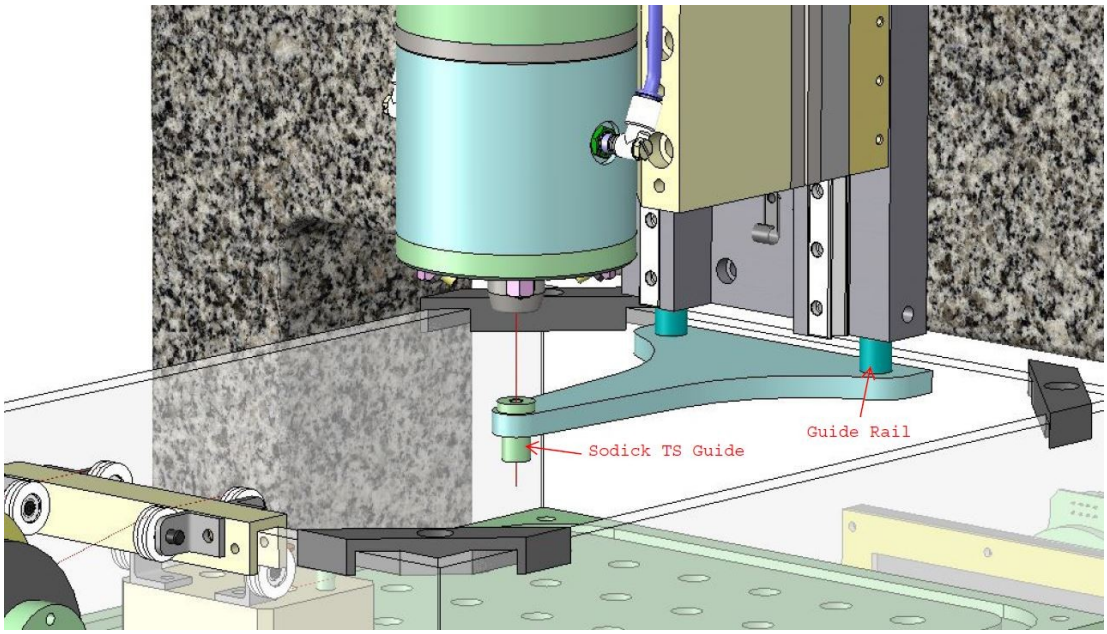

Figure 3.41: Deep hole drilling guide

panel mounted option and how it may be incorporated into the machine platform. Figure 3.42 depicts the Tescom system on the backside of the granite machine base. Figure 3.42 also depicts a pneumatic manifold. The pneumatic manifold contains the three way valves, a regulator, an air dryer and hoses that run to the spindle components. The pneumatic manifold can be bolted directly into the granite structure by using threaded inserts that are adhered into holes drilled into the granite.

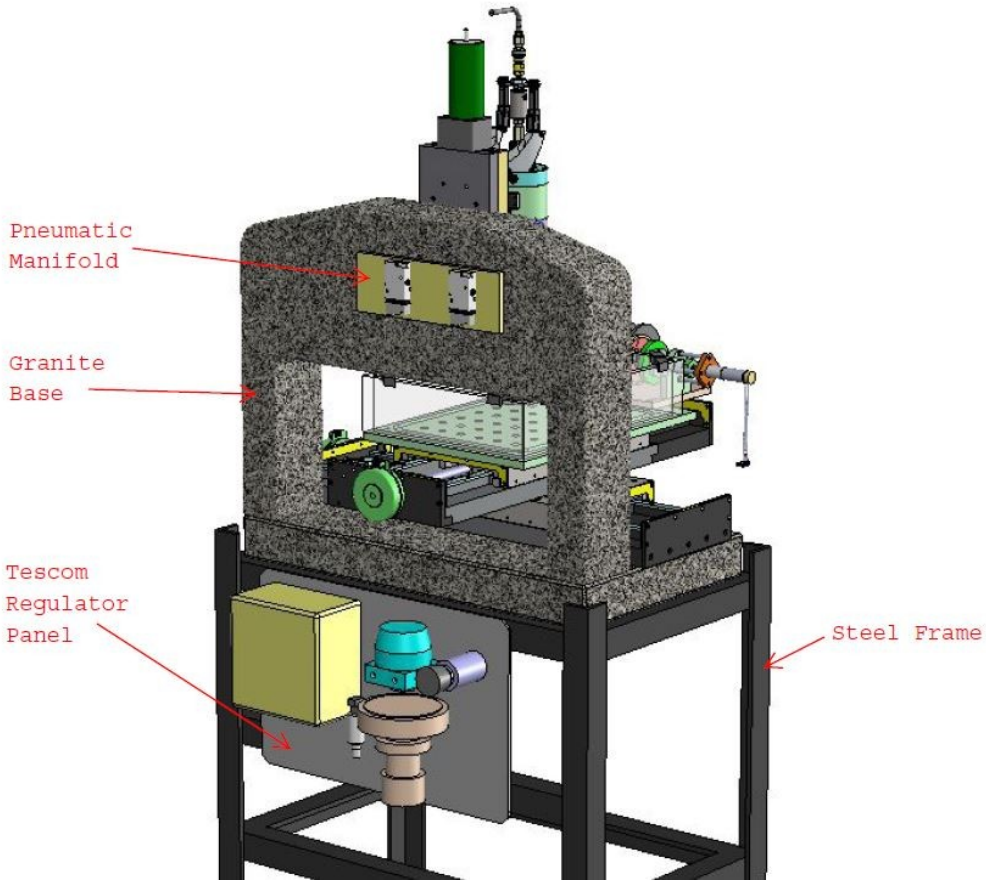

Figure 3.42: Mounted regulator kit

CHAPTER 4

MANUFACTURING OF KEY COMPONENTS

4.1 Spindle Shaft

The goal of the EDM spindle design is accuracy and economy. In order to best achieve these goals the manufacturing process plan for each component needs to be part of the design process. The components are designed to be made from standard tooling and from materials that are relatively easy to machine. The required tolerancing for the precision angular contact bearings is tight, so careful planning of the manufacturing process is required for the spindle shaft and the spindle housing.

The spindle shaft is a critical component in the spindle assembly. The spindle shaft mates with the precision angular contact bearings requiring that the bearing seats on the spindle shaft be precision ground. The bearing seats need to have a precise diameter and be concentric to each other. If the spindle shaft is not manufactured correctly the errors will translate into run out of the electrode, increased bearing friction and reduced bearing life. Figure 4.1 shows the design of the spindle shaft. The light green surfaces are the bearing seats. The shoulders where the bearing inner race contacts the spindle need to be ground in addition to the seats. This shoulder needs to ground to ensure perpendicularity to the seat and inner race. The spindle shaft also contains the closing taper for the 1C collet. The closing taper makes contact with the taper of the 1C

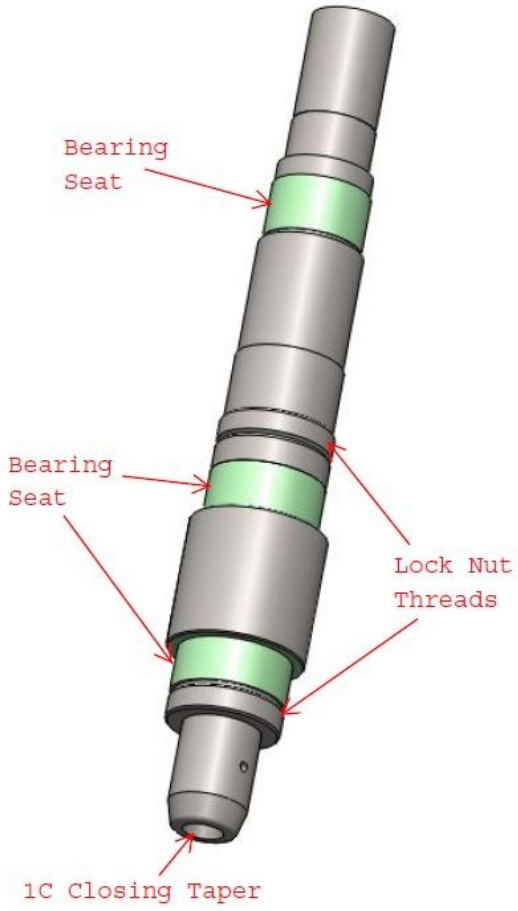

Figure 4.1: Spindle shaft precision features

collet and forces the collet closed as it is drawn up. If the closing taper is not concentric to the bearing seats then the collet and the electrode will run out. For this reason the spindle shaft is designed so that all three bearing seats can be ground in one setup with a live center mating against the closing taper and ensuring concentricity.

The inside of the spindle shaft needs to be drilled out to allow the draw bar to reach the 1C collet. This hole is designed to guide the draw bar and does not require high accuracy but the inner surface needs to smooth for the draw bar guides. This feature can be seen in Figure 4.2 as the draw bar deep hole. In order to achieve a smooth surface finish and a round hole the feature was designed to be reamed. The depth of the reamed

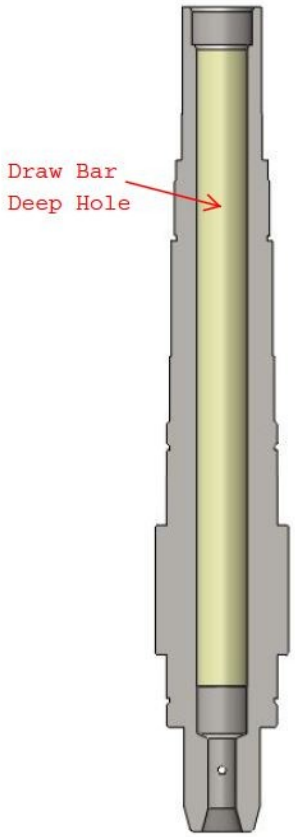

Figure 4.2: Spindle shaft cross section

hole is designed to be bored with a standard length 16 mm reamer while allowing 20 mm of the reamer shank for chucking onto.

The spindle shaft was designed to be made from 17-4 precipitation hardened stainless steel. The spindle shaft is turned on a lathe leaving material where grinding is required then hardened and then ground. The hardening process causes the part distort requiring finish machining. Grinding is a common choice for final machining due its accuracy and ability to machine hard materials.

4.2 Spindle Housing

The spindle housing mates to the outer races of the precision angular contact bearings and like the spindle shaft the housing requires precision grinding to achieve the needed tolerances. The housing is designed so that both of the bearing seats are accessed from one end for machining. This design allows for higher concentricity between the bearings by eliminating re-chucking. Figure 4.3 shows a cross section of the housing design. There is a relief groove in between the bearing seats that minimizes the required grinding and reduces the cost and increases the accuracy. The housing is made from 17-4 stainless steel and is produced in the same way as the spindle shaft. The housing is turned leaving material where grinding is required then hardened and then ground.

The bearing spacer, bearing preload ring and upper bearing cap contact the angular contact bearings and require precision grinding. These components only require

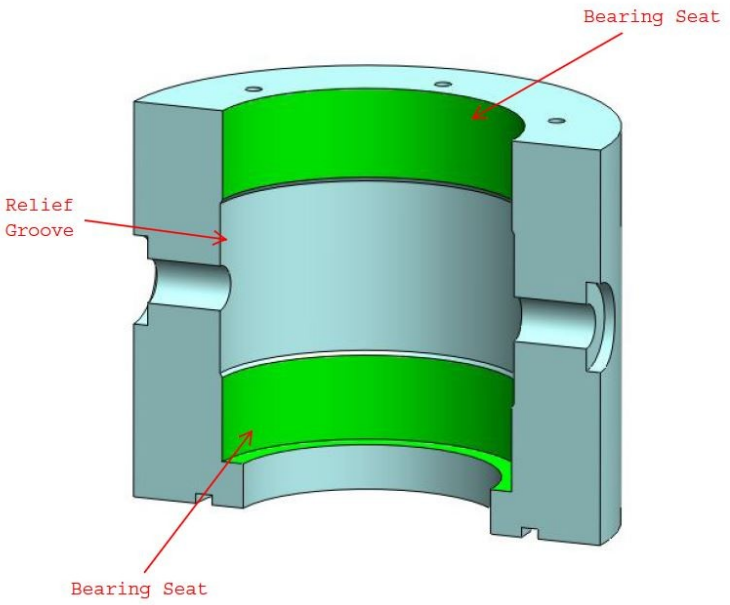

Figure 4.3: Spindle housing cross section

simple surface grinding to meet the flatness requirements needed. The motor housing lid requires some simple cylindrical grinding to house the floating bearing.

4.3 Miscellaneous Machined Components

The V-block was purchased from McMaster-Carr at mcmaster.com as a blank. The desired features of the V-block are then machined. The required machining features include reducing the thickness of the V-block with a face mill and simply adding counterbores and other holes for fixturing. This method allows the use of precision ground 90 degree V that is economical and simple.

The YZ adjust is a flexure that mounts under the V-block. The YZ adjust was designed with a wide and shallow split for a flexure so that the feature could be machined with a standard endmill. The split is 2.4mm wide allowing the feature to be created by a 3/32 in endmill with a 7/16 length of cut. This design eliminates the need for costly Wire EDM machining.

The microgripper Collet is the smallest component that requires machining in the spindle assembly. This collet is designed to be made from 1/8in stainless steel and while the features are relatively small the majority of the part can be made on a lathe. The only features that require special attention are the splits of the collet. The splits are only 0.08mm wide and need to be machined using a Wire EDM. Figure 4.4 shows the microgripper collet and the required splits.

The draw bar and feed tube in the spindle assembly both pose challenges in manufacturing. These two components are long and slender making it extremely difficult to drill or bore the internal diameter. For this reason the draw bar and feed tube are designed to be made from seamless tubing material. The draw bar is 14 mm O.D. by 8.4

Figure 4.4: Microcollet

mm I.D. stainless steel tubing. The feed tube is 8.0 mm O.D. with and I.D. of 3.0 mm. This design allows the feed tube to nicely sleeve inside of the draw bar with little machining. The ends of each component need to be machined but the end features can easily be turned on a lathe with the length of the tubing behind the chuck eliminating the problems associated with cutting long slender components. Figure 4.5 depicts these components and some of the machined features.

At first glance the actuator base mount appears to be a complicated component to manufacture but in reality it is one of the simplest. The mount was designed to be made from aluminum tubing with a 4 inch outer diameter and a 3 inch inner diameter. The outer diameter is turned down to 100 mm while inner diameter is left at 3 inches. The counterbores are then drilled for the fixturing bolts. The final step is to make two 30 degree cuts using a cold saw or miter saw. Figure 4.6 depicts the actuator base mount.

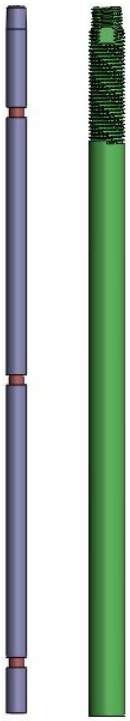

Figure 4.5: Draw bar and feed tube

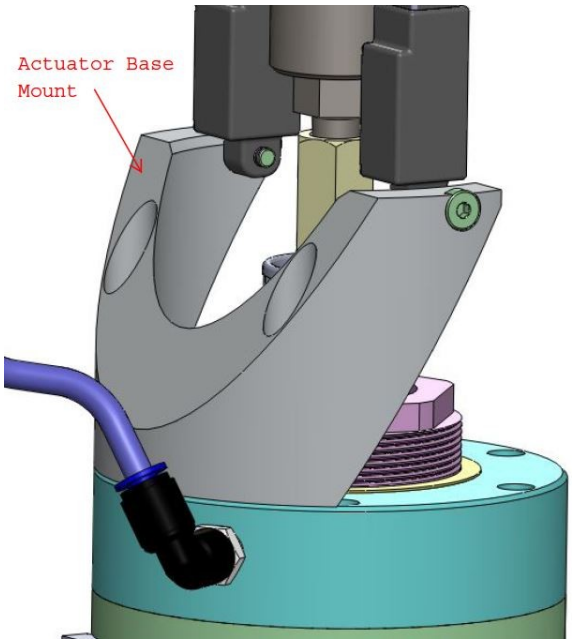

Figure 4.6: Actuator mount base

CHAPTER 5

ASSEMBLY AND ADJUSTMENT

5.1 Fitting and Fixturing Bearings

The assembly of the EDM spindle is of critical importance. If the spindle is assembled improperly then bearing damage, damage of precision components, and electrode run out is likely to occur. The most critical of the assembly procedures are the ones associated with pressing the three ceramic spindle bearings. For this reason the pressing of the spindle bearings is part of the design.

When pressing the bearings it is important to not allow the pressing force to travel through the ceramic rolling elements. If excessive force is applied through the bearing the alloy races can become dimpled or the ceramic rolling elements may fracture. When pressing the inner diameter onto the spindle shaft only the inner race may be contacted. When pressing the outer race into the housing only the outer race may be contacted. When pressing both the inner and outer races simultaneously both races must be contacted and evenly pressed.

The first press performed is pressing the lower angular contact bearing onto the spindle shaft. Figure 5.1 shows this press and the AC Bearing 1 Pressing Tool used to perform the press. This pressing tool ensures that the only the inner race is contacted with a flat surface. It is intended that the press be light enough to be performed with a mallet or dead blow hammer with a hard face. After the bearing is pressed it is secured

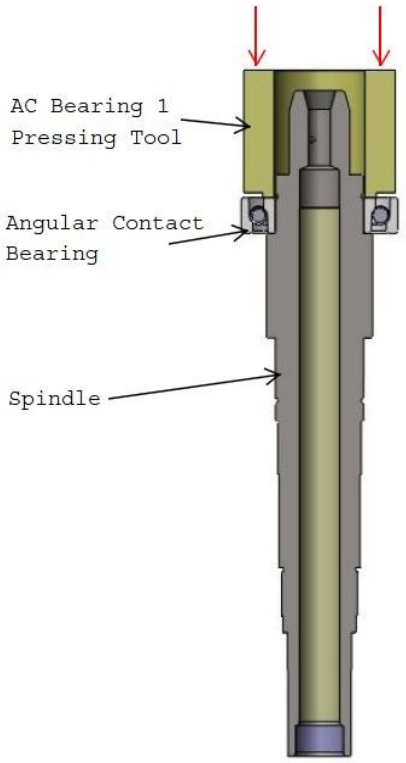

Figure 5.1: Bearing press 1

with a KMK series lock nut to a torque of 20 Nm.

The next step in the assembly is to press the lower angular contact bearing into the Spindle Housing. Figure 5.2 demonstrates this press. In order to perform this press the housing pressing tool 1 was designed to contact the outer races. This tool was designed from a standard tube size to assist in manufacturing. It can be seen in Figure 5.2 that the bearing must pass through the upper housing seat and then into the lower housing seat against a precision ground shoulder.

The next step in the assembly is to install the bearing spacer and the upper angular contact bearing. The bearing spacer simply slips in and rests on top of the outer race of the lower angular contact bearing. The upper angular contact bearing is then pressed

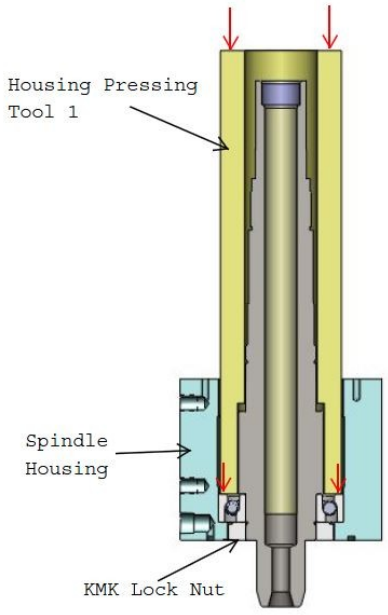

Figure 5.2: Bearing press 2

onto the spindle shaft and into the housing simultaneously. Figure 5.3 depicts this press and the tools required. The housing pressing tool 2 is used to press onto the inner and outer races of the upper angular contact bearing while the tool is gently tapped down. In order to not pass high loads through the lower bearing support tooling must be used. To serve this purpose housing anvil_1 and housing anvil_2 were designed.

Housing anvil_1 supports the housing and the forces that are applied to the outer race of the upper angular contact bearing. Housing anvil_2 supports the spindle shaft and the forces applied to the inner race of the upper angular contact bearing. It is important that the two anvil tools contact both the spindle and housing at the same time. In order to achieve the correct height shims may need to be placed under one of the tools.

The next step in the assembly is to fixture the upper angular contact bearing and apply preload to the bearings. The upper bearing cap is used to fixture the outer race.

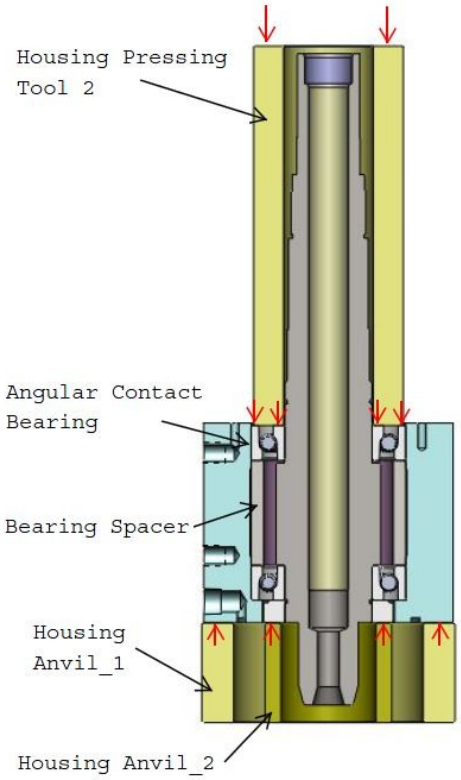

Figure 5.3: Bearing press 3

The upper bearing cap is pulled down onto the outer race of the bearing by six M4 bolts torqued to 0.64 Nm. This fixturing force is pressed through the bearing spacer and fixtures the outer race of the lower angular contact bearing. The preload is applied using the KMK preload nut and preload ring. The preload ring is used to space up the lock nut so that it can be accessed with a hook spanner wrench. The KMK preload lock nut is torqued to 0.3 Nm to provide a preload force of 60 N. This preload force is the minimum required for proper function of the bearings and provides a long bearing life. The calculation used to determine the minimum preload force is covered in Chapter 6 subsection 6.6. Figure 5.4 depicts the fixturing arrangement used to preload and secure the bearings. The KMK preload lock nut is secured using a spanner wrench.

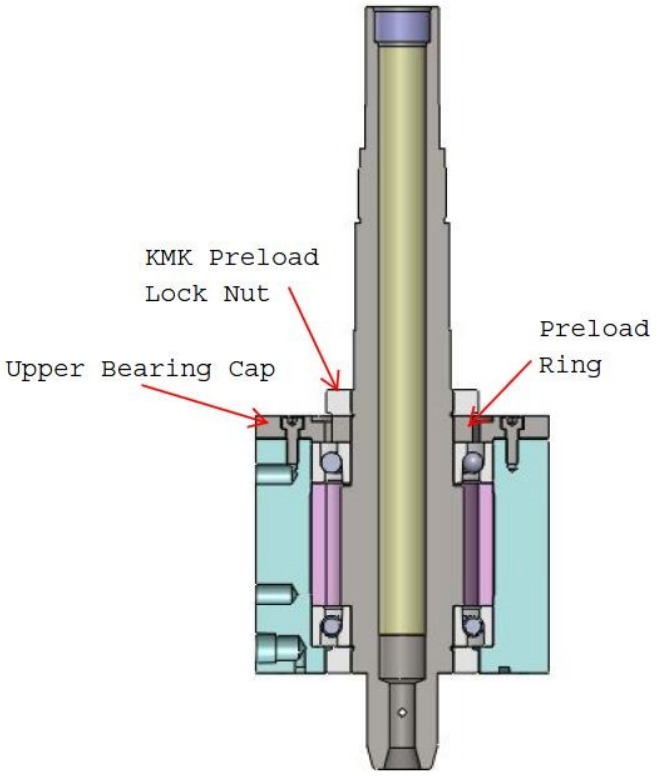

Figure 5.4: Bearing press 4

The final bearing press is for the deep groove radial ball bearing. This bearing's inner race is pressed onto the spindle shaft while the outer race of the bearing floats in the motor housing lid. Figure 5.5 shows how the bearing is pressed onto the spindle shaft. The radial bearing pressing tool is used to tap the radial ball bearing onto the spindle shaft. The bearing is placed axially with a snap ring and an abutment collar. In order to avoid putting pressing loads through the upper angular contact bearing the housing anvil_2 must be used to support the spindle shaft.

5.2 Closer Preload Adjustment

Each time the 1C collet is changed the draw bar must be adjusted. This is done by grasping the draw bar handle and rotating it to unthread the draw bar from the 1C collet.

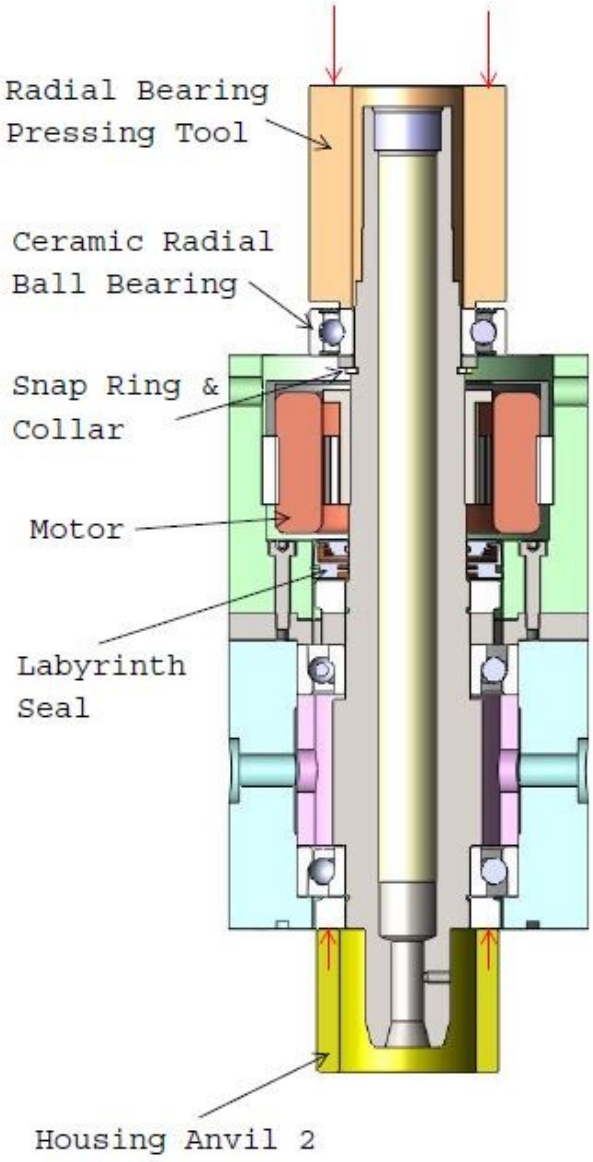

Figure 5.5: Bearing press 5

The handle was designed to be comfortably grasped with knurling to assist in gripping. Figure 5.6 depicts the draw bar handle and its surroundings in the spindle. The draw bar handle is made from an acetal which insulates the operator from shock. The machine platform should be set up with a door switch to keep the operator away from a live spindle but since the operator is intended to touch the draw bar handle it is an added precaution.

The 1C collet is loaded by first setting the closer in an open state. The 1C collet is then aligned with the key slot in the collet to the spindle key. The 1C collet is then pressed into the spindle until it contacts the threaded draw bar insert. The draw bar handle is then turned threading the 1C collet up into the spindle closing taper. This is continued until the 1C collet lightly grasps the electrode. The draw bar handle is then

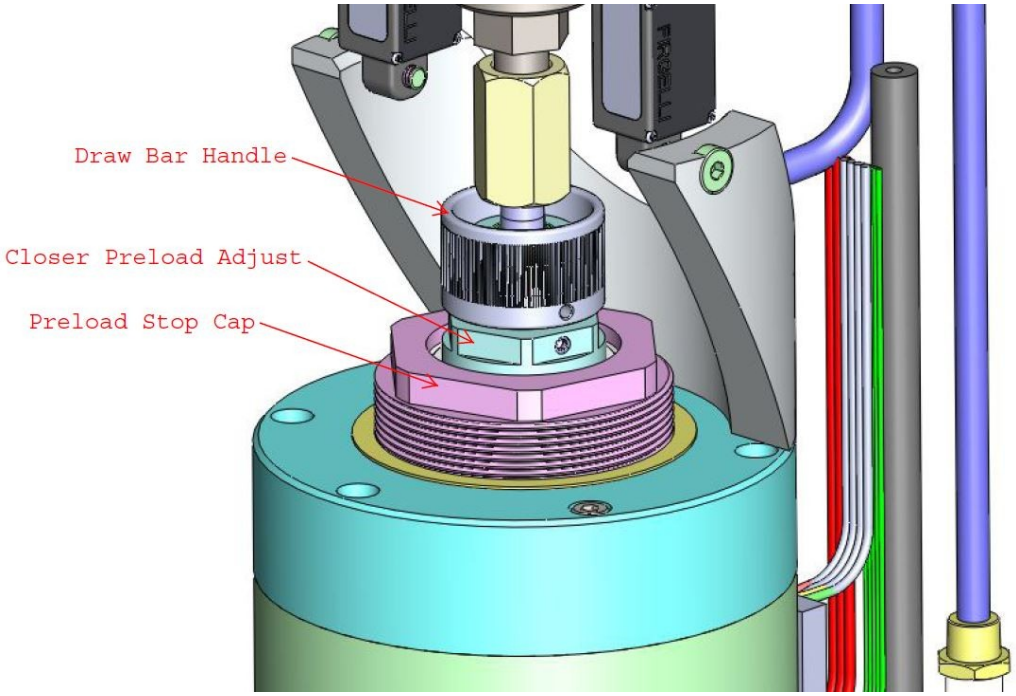

Figure 5.6: Closer preload adjustment

backed off a quarter to a half of a turn to ensure electrode clearance through the collet. The draw force is adjustable and can be set to accommodate the electrode being used. The thin walled brass or copper tubing will need a much lower force than an electrode made of tungsten or with a solid core. The draw is a simple adjustment and can be performed quickly. The first step is back the preload stop cap off the closer preload adjust by unthreading it a half turn. The combined wrench can then be used to adjust the preload stop cap and preload adjust simultaneously. Once the desired draw is reached the closer preload adjust is fixed with a set screw and the preload stop cap is threaded back down onto the closer preload adjust. The draw system was designed to be able to load one of two draw springs. The ability to use different draw springs allows for a greater range of draw forces. There is a light draw spring which provides a maximum draw of 273 N with a spring constant of 20 N/mm. The heavy draw spring provides a maximum draw of 377 N with a spring constant of 37 N/mm. The heavy spring provides a higher maximum draw force while the light spring provides a finer adjustment.

5.3 Loading an Electrode

The loading of an electrode into the spindle will need to be done regularly as the old electrode wears down too short or when a different type of electrode is required. For this reason the loading of an electrode needs to be simple and able to be performed quickly by an operator. The electrode is changed in the current design with only a few simple steps. First the operator disconnects the dielectric line. This is done easily with the use of the quick connect fitting. Then the two thumb nuts on top of the linear actuators are removed. These nuts are tightened and loosened by hand allowing the operation to be performed quickly. After removing the thumb nuts the rotary union, feed

tube, and microgripper are all free to come out as one assembly. Once the assembly has been removed a new electrode can be fed into the microgripper and feed tube. The assembly is then placed back into the spindle in the reverse order. The components involved with changing the electrode are depicted in Figure 5.7.

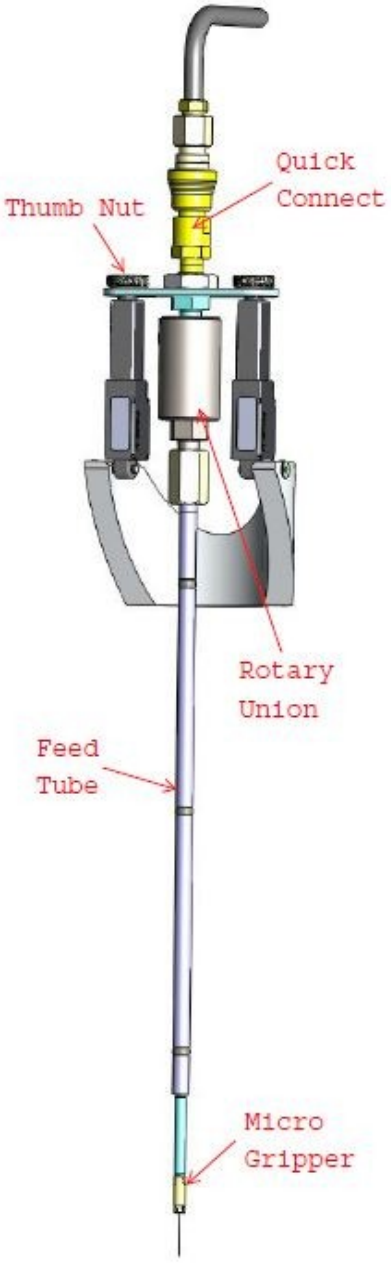

Figure 5.7: Feed tube assembly

CHAPTER 6

ANALYTICAL INVESTIGATION

6.1 Exit Velocity of Dielectric Fluid

Several aspects of the spindle design presented unknowns in the design characteristics. For these instances an analytical analysis is performed to give an estimate of the spindle performance. These instances include the exit velocity of the dielectric, spindle deflection, bearing stiffness, bearing life, max allowable closing force for both collets, and deflection of the YZ adjust.

The dielectric exit velocity is an important parameter in EDM machining. An exit velocity that is too low will fail to remove EDM debris while an exit velocity that is too high may cause turbulence in the discharge gap which results in damage to the workpiece. The exit velocity is affected by pressure, electrode length, and the electrode's inner diameter so it is critical to be able to determine the exit velocity based on these given parameters. An important characteristic of the fluid flow problem is whether or not the flow is laminar or turbulent. In order to determine this, Equation 6.1 below is used [30].

$$Re = \frac{\rho \overline{V} D}{\mu} \tag{6.1}$$

where Re is the Reynolds number, ρ is the fluid density, $\overline{V}$ is the average flow velocity, D

is the inner pipe diameter and μ is the fluid viscosity. The flow in a pipe will be generally laminar if the Reynolds number is below 2300. For this reason the Reynolds number is set to 2300 and the resulting average flow velocity is determined. The EDM spindle is designed to primarily use the 0.25 mm tubular electrode with an inner diameter of 0.10 mm with a length of 400 mm. For this reason the calculations are based off of this tube size. For this tube the diameter in Equation 1 will be 0.10 mm. Water is used for the dielectric fluid and its properties are used in Equation 1. The density of water is 998 kg/m^3. The viscosity of water at room temperature is 1.002x10^{-3} N·s/m^2. Using Equation 1 it was determined that an average flow velocity of 23 m/s will result with a Reynolds number of 2300. Since an exit velocity of 23 m/s is well above the intended exit velocity it is assumed that the flow will be laminar. Given a laminar flow the analysis can be continued.

The pressure drop can be determined as a function of flow rate using Equation 6.2.

$$\Delta p = \frac{Q*128*\mu*L}{\pi*D^4} \tag{6.2}$$

where Δp is the pressure drop, Q is the flow rate, and L is the length of the electrode. The flow rate is determined from Equation 6.3.

$$Q = \overline{V} * A \tag{6.3}$$

where A is the cross sectional area of the tube's inner diameter. Using Equations 6.2 and 6.3 the average flow velocity can be determined from the electrode's length. Using 1000 psi of dielectric pressure and 400 mm of electrode length the anticipated exit velocity is

5.4 m/s. By the time the electrode is worn down to its shortest length of 14 mm the pressure will have to be reduced to 35 psi to maintain the 5.4 m/s exit velocity.

6.2 Bearing Stiffness Approximation

In order to optimize the stiffness of the spindle assembly and anticipate spindle deflections the stiffness of the bearings needs to be determined. Most bearing manufacturers provide axial stiffness values of the bearings but rarely provide the radial stiffness of the bearings. This is due to the fact that the radial stiffness of the bearing depends on the effects of preload, radial load, rotational velocity, and temperature for the given application. In order to obtain a value for the radial bearing stiffness an analytical approximation is used. This approximation determines the radial stiffness based upon the radial load, the rolling element diameter, the number of rolling elements, and the contact angle of the bearing. This approximation can be seen as Equation 6.4.

$$\frac{K_{xx}}{d^{1/3}n^{2/3}cos^{5/3}\beta} = 3.247 * 10^4 * F_{xx} \tag{6.4}$$

where K_{xx} is the radial stiffness, d is the roller diameter, n is the number of rollers, β is the contact angle and F_{xx} is the applied radial load. The contact angle of the angular contact bearings is 15 degrees. The bearing contains 17 rolling elements with a diameter of 3.57 mm. The applied radial load is provided through the axial preload and the weight of the inner spindle components and comes out to 174 N. Using Equation 6.4 the radial stiffness of the angular contact bearings is estimated at 62.6 N/µm. SKF recommends a correction factor of 1.11 to account for the added stiffness of the silicon nitride rolling elements, yielding an estimated radial stiffness of 69.5 N/µm.

The stiffness of the deep groove radial ball bearing located at the top of the

spindle shaft also needs to be determined. Equation 6.4 can also be used to approximate the radial stiffness of a radial ball bearing by simply using a zero degree contact angle. The radial ball bearing chosen is the SKF 6006-2RZTN9. This hybrid bearing contains 11 rolling elements with a diameter of 3.57 mm. The applied radial load is estimated at 50 N and is produced by the press fit of the inner race. Using Equation 6.4 and a 1.11 correction factor it was determined that the radial stiffness of the deep groove radial ball bearing is 36.4 N/μm.

The axial stiffness of the angular contact bearings is provided by SKF for a back to back configuration with a light preload. The axial stiffness was found to be 40.0 N/μm [26]. The axial stiffness of the deep groove radial ball bearing is neglected since this bearing floats in its housing and is not designed to provide thrust loads.

6.3 Spindle Stiffness

Now that the bearing stiffness has been approximated the stiffness of the spindle assembly can be determined. The spindle housing and mount is assumed to have an infinite stiffness and does not contribute to deflection of the spindle shaft. Therefore only the spindle shaft and bearings are analyzed for deflection. Figure 6.1 depicts a free body diagram of the spindle shaft. The spindle shaft is analyzed as an Euler-Bernoulli beam and the bearings are approximated as linear springs with a spring constant equal to the radial stiffness of each bearing.

The beam depicted in Figure 6.1 is statically indeterminate due to the three reaction forces. There are three unknown reactions and only two equations of static equilibrium to solve for them. The spring supports allow for both deflection and slope of the beam. In order to determine the reaction forces Castigliano's theorem is used to

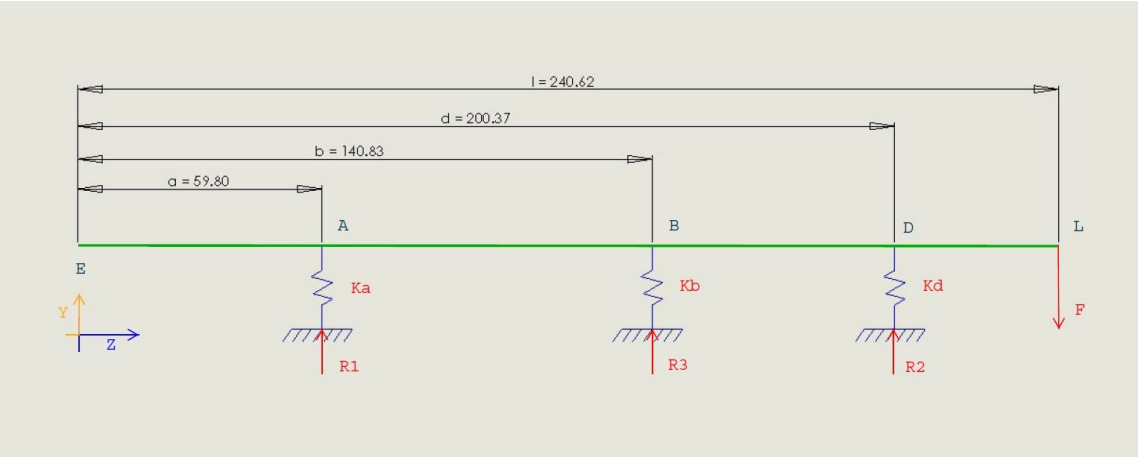

Figure 6.1: Free body diagram

account for the elastic energy absorbed by the supports. Castigliano's theorem states that the displacement of a point in the beam is equal to the first partial derivative of the strain energy with respect the force acting at that point [31]. Castigliano's theorem is expressed as Equation 6.5.

$$q_i = \frac{\partial U}{\partial F_i} \tag{6.5}$$

where q_i is the deflection at i, U is the internal strain energy and F_i is the force at i in the direction of the deflection. When using Castigliano's theorem to solve indeterminate beams one of the reaction forces is set to be redundant, allowing for the deflection with respect to this force to be set to zero [32]. This relationship is expressed in Equation 6.6.

$$0 = \frac{\partial U}{\partial R} \tag{6.6}$$

where U is the strain energy, and R is the redundant force. Equation 6.6 provides another equation in addition to the equations of static equilibrium and allows for unknown

reactions to be determined. The spindle shaft is considered to be a slender beam and thus the effects of shear and axial elongation on the strain energy is neglected as its effects are small compared to the effects of the moment. Thus the strain energy for the beam is defined in Equation 6.7 as

$$U = \int_0^l \frac{M^2 dx}{2EI} \tag{6.7}$$

where M is the internal moment of the beam, E is the modulus of elasticity of beam material, and I is the moment of inertia of the beam's cross section.

The spring supports also contain strain energy which needs to be accounted for when performing the analysis. The strain energy of a simple spring is given in Equation 6.8 as

$$U = \frac{1}{2} k \delta^2 \tag{6.8}$$

where k is the spring constant, and δ is the deflection of the spring. The deflection of the spring can be determined from the applied force and the spring constant. Equation 6.9 below follows as

$$\delta = \frac{F}{k} \tag{6.9}$$

where F is the applied force. Using this definition Equation 6.8 can be rewritten as

$$U = \frac{F^2}{2k} \tag{6.10}$$

The following analysis is performed using the free body diagram in Figure 6.1.

The unknown reaction forces R_1, R_2, and R_3, are determined using a balance of the forces in the *Y* direction, a balance of the moments at point *A* and from a balance of the strain energy. This gives three unknowns and three governing equations allowing for a solution of the indeterminacy. A static balance of the forces in the *Y* direction follows as

$$\sum F_y = 0 = R_1 + R_2 + R_3 - F \tag{6.11}$$

Equation 6.11 can be rewritten as follows.

$$R_1 = F - R_2 - R_3 \tag{6.12}$$

A static balance of the moments at point *A* follows as

$$\sum M_A = 0 = R_3(b - a) + R_2(d - a) - F(l - a) \tag{6.13}$$

Now the energy balance begins by defining the strain energy of the beam and support deflections. This balance follows as

$$U = \int_0^a \frac{M^2}{2EI} dz + \int_a^b \frac{M^2}{2EI} dz + \int_b^d \frac{M^2}{2EI} dz + \int_d^l \frac{M^2}{2EI} dz + \frac{{R_1}^2}{2k_a} + \frac{{R_2}^2}{2k_d} + \frac{{R_3}^2}{2k_b} \tag{6.14}$$

where k_a, k_b , and k_d are the spring constants of the supports. The supports are the three bearings approximated as springs with a spring constant equal to the bearing's radial stiffness. The first four terms of Equation 6.14 account for strain energy of the beam. The energy of the beam is calculated in four sections as the equation of internal moment changes between supports. The last three terms of Equation 6.14 account for the energy associated with the deflection of the spring supports. Equations 6.15 to 6.18 give the internal moments in each section of the beam.

$z \leq a$: $M_0 = 0$ (6.15)

$a \leq z \leq b$: $M_1 = R_1(z - a)$ (6.16)

$b \leq z \leq d$: $M_2 = R_1(z - a) + R_3(z - b)$ (6.17)

$d \leq z \leq l$: $M_3 = R_1(z - a) + R_3(z - b) + R_2(z - d)$ (6.18)

Using the positions of the supports seen in Figure 6.1 and Equations 6.14 through 6.18 the total strain energy can be expressed as Equation 6.19.

$$U = \int_0^a \frac{0^2}{2EI} dz + \int_a^b \frac{(R_1(z-a))^2}{2EI} dz + \int_b^d \frac{(R_1(z-a)+R_3(z-b))^2}{2EI} dz + \int_d^l \frac{(R_1(z-a)+R_3(z-b)+R_2(z-d))^2}{2EI} dz + \frac{{R_1}^2}{2k_a} + \frac{{R_2}^2}{2k_d} + \frac{{R_3}^2}{2k_b} \quad (6.19)$$

Now setting R_2 as the redundant force, Equation 6.6 becomes.

$$\frac{\partial U}{\partial R_2} = 0 \quad (6.20)$$

Using Equations 6.12, 6.19 and 6.20 along with the support positions seen in the free body diagram, the partial derivative of the internal energy with respect to the redundant force can be written as

$$\frac{\partial U}{\partial R_2} = 0 = \frac{(177344(R_2+R_3-F)+748540*R_2+534558*R_3-748540*F+748540*R_2+534558*R_3-748540*F}{2EI} + \frac{-(F-R_2-R_3)}{2k_a} + \frac{R_2}{k_d} \quad (6.21)$$

Now using the modulus of elasticity and moment of inertia for the spindle's cross section, Equation 6.21 can be simplified into Equation 6.22. In order to simplify the calculations, the spindle shaft was approximated as having a constant cross sectional area and moment of inertia. A more precise estimate of the support reactions would require that each section of the spindle shaft be given a unique moment of inertia as the inner and outer diameters of the spindle shaft vary.

$$\frac{\partial U}{\partial R_2} = 0 = 0.000168 * R_2 + 0.000114 * R_3 - 0.000162 * F \tag{6.22}$$

Equations 6.22 and 6.12 form a two by two system with two equations and two unknowns, R_2 and R_3. Once the two by two is solved the values of R_2 and R_3 are used in Equation 6.12 two yield the result for all three reaction forces.

$$R_2 = 3.104 * F \tag{6.23}$$

$$R_3 = -3.153 * F \tag{6.24}$$

$$R_1 = 1.049 * F \tag{6.25}$$

Now that the reaction forces have been determined, the deformation of the beam can be calculated. The slope and displacement of the beam was determined using the integration method. This method derives from the flexure formula and is used to determine the curvature of the beam with an applied moment. Equation 6.26 expresses this relationship.

$$EI\frac{d^2q}{dz^2} = M(z) \tag{6.26}$$

In this equation q is the deflection of the beam and its second derivative is the curvature of the beam. *M(z)* in Equation 6.26 is the internal moment of the beam and is a function of z. The moment in the beam has already been defined in equations 15 through 18 and 23 through 25. The deflection is calculated in each section of the beam between the supports. The first analyzed is the section between points *A* and *B* denoted as section one. Using Equation 6.26 the curvature in section one follows as

$$EI\frac{d^2q_1}{dz_1{}^2} = 1.049 * F * z_1 - 62.746 * F \tag{6.27}$$

Now Equation 6.27 can be integrated twice to yield the desired deflection q_1

$$EI\frac{dq_1}{dz_1} = \frac{1.049*F*z_1{}^2}{2} - 62.746 * F * z_1 + C_1 \tag{6.28}$$

$$EI * q_1 = \frac{1.049*F*z_1{}^3}{6} - \frac{(62.746*F*z_1{}^2)}{2} + C_1 * z_1 + C_2 \tag{6.29}$$

where C_1 and C_2 are constants of integration and need to be solved for. Equation 6.29 provides the deflection of the beam in section one and Equation 6.28 provides the slope of the beam in section one. The same procedure is applied to sections two and three to provide the following equations.

$$EI * q_2 = \frac{1.049*F*z_2{}^3}{6} - \frac{62.746*F*z_2{}^2}{2} - \frac{3.153*F*z_2{}^3}{6} + \frac{44.07*F*z_2{}^2}{2} + C_3 * z_2 + C_4 \tag{6.30}$$

$$EI * q_3 = \frac{1.049*F*z_3{}^3}{6} - \frac{62.746*F*z_3{}^2}{2} - \frac{3.153*F*z_3{}^3}{6} + \frac{44.07*F*z_3{}^2}{2} + \frac{3.10398*F*z_3{}^3}{6} - \frac{621.94*F*z_3{}^2}{2} + C_5 * z_3 + C_6 \tag{6.31}$$

The constants of integration introduce six unknowns in equations 6.29 through 6.31. To determine these values, boundary conditions need to be used. Six boundary conditions are used to provide the six needed equations to solve for the constants of integration. The first boundary condition states that the deflection at point *A* of the beam is equal to the deflection of the spring support at *A*. This relationship is can be seen in the following equation as

$$q_1(A) = \frac{R_1}{k_a} \tag{6.32}$$

where $q_1(A)$ is the deflection of section one at point *A*. The second boundary condition states that the deflection of section one at point *B* is equal to the deflection of the spring support at *B*.

$$q_1(B) = \frac{R_3}{k_b} \tag{6.33}$$

The third boundary condition states that the deflection of the beam in section two at point *B* is also equal to the deflection of the spring support at *B*.

$$q_2(B) = \frac{R_3}{k_b} \tag{6.34}$$

The fourth boundary condition states that the deflection of the beam at point *D* is equal to the deflection of the spring support at *D*.

$$q_2(D) = \frac{R_2}{k_d} \tag{6.35}$$

The fifth boundary condition states that the deflection of the third beam section at point *D* is equal to the deflection of the spring support at *D*.

$$q_3(D) = \frac{R_2}{k_d} \tag{6.36}$$

The sixth and final boundary condition states that the slope of section 2 and section 3 are equal to one another at point *D*.

$$\frac{dq_2(D)}{dz_2} = \frac{dq_3(D)}{dz_3} \tag{6.37}$$

Using equations 6.32 through 6.37 the six constants of integration may be simultaneously solved to provide the solutions.

$$C_1 = -11723.8 * F \tag{6.38}$$

$$C_2 = 1.168 * 10^6 * F \tag{6.39}$$

$$C_3 = -13576.5 * F \tag{6.40}$$

$$C_4 = -1.507 * 10^6 * F \tag{6.41}$$

$$C_5 = 48732.1 * F \tag{6.42}$$

$$C_6 = -5.668 * 10^6 * F \tag{6.43}$$

Using these solutions Equations 6.29, 6.30, and 6.31 become

$$EI * q_1 = \frac{1.049*F*{z_1}^3}{6} - \frac{(62.746*F*{z_1}^2)}{2} - 11723.8 * F * z_1 + 1.168 * 10^6 * F \tag{6.44}$$

$$EI * q_2 = \frac{1.049*F*{z_2}^3}{6} - \frac{62.746*F*{z_2}^2}{2} - \frac{3.153*F*{z_2}^3}{6} + \frac{44.07*F*{z_2}^2}{2} - 13576.5 * F * z_2 - 1.507 * 10^6 * F \tag{6.45}$$

$$EI * q_3 = \frac{1.049*F*{z_3}^3}{6} - \frac{62.746*F*{z_3}^2}{2} - \frac{3.153*F*{z_3}^3}{6} + \frac{44.07*F*{z_3}^2}{2} + \frac{3.10398*F*{z_3}^3}{6} -$$

$$\frac{621.94*F*{z_3}^2}{2} + 48732.1 * F * z_3 + -5.668 * 10^6 * F \quad (6.46)$$

Equations 6.44, 6.45, and 6.46 give the deflection of the beam in sections one, two and three.

Now all that remains is to determine the deflection of the beam in section zero. Section zero is the section of beam from the free end to the first support at point *A*. As can be seen from Equation 6.15 there is no moment in this section of the beam so it has no curvature, however, it does still have deflection. Using Equation 6.26 the curvature can be written as

$$EI\frac{d^2q_0}{d{z_0}^2} = 0 \quad (6.47)$$

Integrating Equation 6.47 twice provides the slope and deflection in beam section zero.

$$EI * \frac{dq_0}{dz_0} = C_0 \quad (6.48)$$

$$EI * q_0 = C_0 * z_0 + C_\alpha \quad (6.49)$$

Boundary conditions are now applied to solve for the constants of integration. Equation 6.49 is the equation of a line with a slope of C_0 and a y intercept value of C_α/EI. The slope C_0/EI is the same as the slope at the support at point *A*. The slope at point *A* in section one is determined using Equation 6.28 and follows as

$$\frac{dq_1(a)}{dz_1} = \frac{dq_0}{dz_0} = \frac{C_0}{EI} = \frac{1.049*F*a^2}{2EI} - \frac{62.746*F*a}{EI} - \frac{11723.8*F}{EI} \quad (6.50)$$

Now the slope C_0/EI has been determined and only the y intercept C_α/EI needs to be determined. The y intercept is the deflection at z=0 and can be found from the beam deflection at point A and the slope C_0/EI

$$\frac{C_\alpha}{EI} = \frac{R_1}{k_a} - \frac{C_0}{EI} * a \tag{6.51}$$

The deflection of the beam from the free end up to the first support can now be written as

$$q_0 = \left(\frac{1.049*F*a^2}{2EI} - \frac{62.746*F*a}{EI} - \frac{11723.8*F}{EI}\right) * z_0 + \frac{R_1}{k_a} - \left(\frac{1.049*F*a^2}{2EI} - \frac{62.746*F*a}{EI} - \frac{11723.8*F}{EI}\right) * a \tag{6.52}$$

Now the deflection of the entire beam can be determined from a given force applied at the end. The deflection resulting from an applied force is given in Figure 6.2. The applied force F in Figure 6.1 is 100 N and results in a maximum deflection of 0.01 mm at the loaded end of the shaft. Figure 6.2 shows an exaggerated view of the deflection so that it may be easily seen. The reaction forces are also depicted in Figure 6.2. The

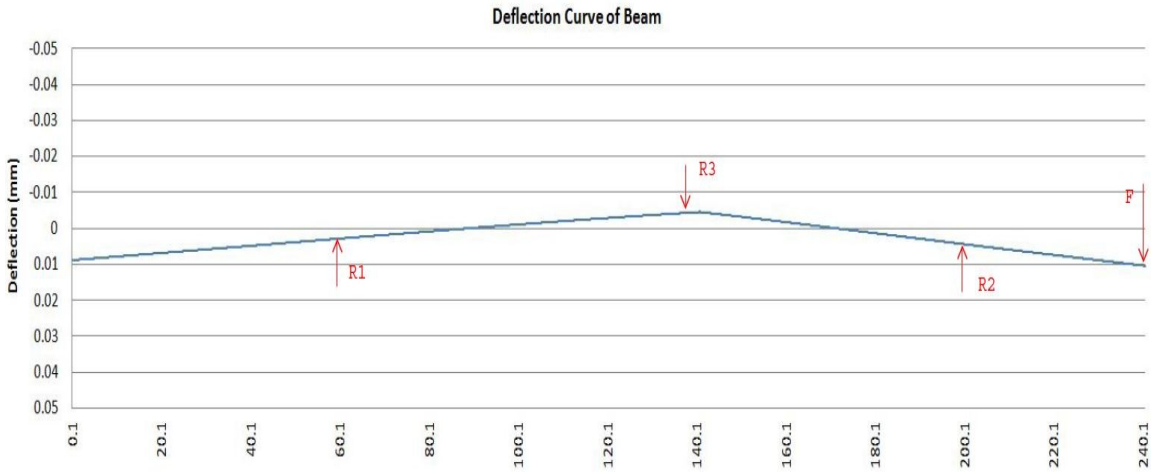

Figure 6.2: Spindle shaft deflection

reaction forces are shown in their locations along the spindle and the direction of the forces are shown.

6.4 Bearing Life

The spindle bearings will continuously rotate for long periods of time while machining. The long machining interval warrants an investigation of the bearing's life expectancy. The equation used for this purpose follows as

$$L_{10} = (\frac{C}{P})^3 \tag{6.53}$$

where L_{10} is the basic rating life with 90% reliability, C is the dynamic load rating and P is the equivalent dynamic load. The dynamic load rating is provided by the manufacturer but the equivalent dynamic load must be calculated. The equivalent dynamic load is a single load acting in the radial direction that has the same influence on bearing life as the combined actual loads. Figure 6.3 from SKF provides a graphical depiction of this concept. For determining the equivalent dynamic load Equation 6.54 is used

$$P = X * F_r + Y * F_a \tag{6.54}$$

where F_r is the applied radial load, F_a is the applied axial load, X is the radial load factor and Y is the axial load factor. The load factors are provided by the manufacturer allowing for simple calculation. For the given spindle application there are no applied radial loads and the axial load factor is equal to 1.47. The axial load is provided form the preload and the weight of the supported components. The axial load is 80 N and provides an equivalent dynamic load of 118 N. The bearing life calculation now follows as

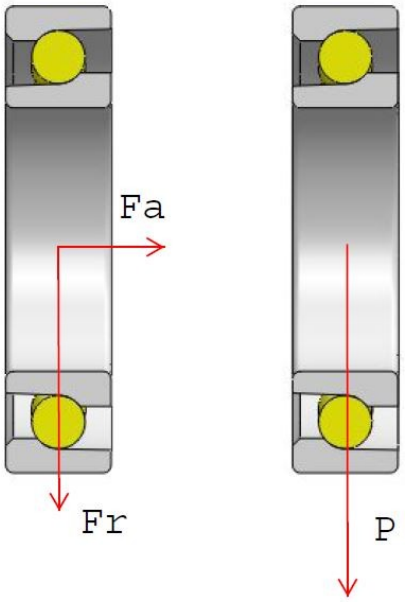

Figure 6.3: Equivalent loading [Adapted from 29]

$$L_{10} = (\frac{15.6\ kN}{118})^3 = 2.33x10^6\ million\ revolutions$$

equivalent dynamic load of 118 N. The bearing life calculation now follows as

$$L_{10} = (\frac{15.6\ kN}{118})^3 = 2.33x10^6\ million\ revolutions$$

In order to complete this number of revolutions the spindle would have to rotate at 1000 rpm for 4400 years.

6.5 Minimum Bearing Load

The long bearing life is due to the extremely low applied forces, however, in order for the bearing to function properly a minimum force must be applied. Since the loads are small in the spindle application it is important to ensure that the minimum load has

been reached. SKF has provided an equation for calculating the minimum load which follows as

$$F_{rm} = k_r * (\frac{\nu * n}{1000})^{2/3} * (\frac{d_m}{1000})^2 \quad (6.55)$$

where F_{rm} is the minimum radial load, k_r is the minimum load factor, ν is the lubricating oil viscosity, n is the rotational speed and d_m is the mean diameter of the bearing. The minimum load factor is provided from the manufacturer as 0.083 and the viscosity of the oil is 7 mm^2/s. Using these data Equation 6.55 yields a minimum radial load of 71.5 N. It is now known that the minimum load has been reached since the equivalent dynamic load provided by the preload was already determined to be 118 N.

6.6 Tightening Torque for Bearing Fixturing

In order to properly fixture the bearings the correct tightening torques for the precision lock nuts and end cap bolts must be calculated. When clamping the lock nut down on the lower angular contact bearing's inner race the tightening torque if found by

$$M_t = K[F_s + (N_{cp} * F_c) + G_{A,B,C}] \quad (6.56)$$

where M_t is the tightening torque, F_s is the minimum axial clamping force, N_{cp} is the number of preloaded bearings, F_c is the axial fitting force, K is the calculation factor dependent on the locking threads, and $G_{A,B,C}$ is the built in bearing preload prior to mounting. The minimum axial clamping force F_s and axial fitting force F_c are provided from SKF as 3300 N and 750 N. SKF also provides the calculation factor K for the M35 lock nut as 4.5. Using these bearing data the tightening torque is determined to be 20 Nm.

The tightening torque for the preload lock nut is also determined using Equation 6.56. The axial preload required for the spindle is 60 N. The tightening torque for the preload then follows as 0.3 Nm.

The upper bearing cap clamps the outer race of both the angular contact bearings. The upper bearing cap is fixtured with six M4 socket head cap screws. Since these bolts provide the clamping force for fixturing the bearings the correct tightening torque for the bolts needs to be determined. This is done using Equation 6.56 and dividing by the number of bolts. For an M4 bolt the calculation factor *K* is 0.8. Evaluating Equation 6.56 and dividing by six produces a tightening torque of 0.64 Nm per bolt.

6.7 Angular Accuracy of C-Axis

In order to determine the expected angular positioning accuracy the resolution of the rotary encoder is investigated. The rotary encoder has 2400 counts per revolution and dual channel quadrature signal allowing for the controller to increase the resolution four times. Since some error is expected the accuracy is multiplied by five. It is a good rule of thumb to design the machine accuracy 2-5 times the encoder resolution [33]. The angular accuracy then becomes

$$A_a = 5 * \frac{360°}{4*2400cpr} \tag{6.57}$$

where A_a is the angular accuracy. Equation 6.57 is evaluated to produce an angular accuracy of 0.19 degrees.

6.8 Max Gripping Force of 1C Collet

In order to anticipate the needed gripping forces of the 1C collet and microcollet the strength of the electrode and gripping characteristics need to be analyzed. The maximum closing force is designed to be more than enough to yield the standard copper electrode used, with an outer diameter of 250 μm and an inner diameter 125μm. In order to provide a simple estimate of the attainable gripping force the electrode is analyzed as if it were in hydrostatic stress. To evaluate the stress in the electrode cylinder the Lamé solution is used. The Lamé solution follows as

$$\sigma_r = p_i * \frac{b^2}{a^2-b^2} * \left(1 - \frac{a^2}{r^2}\right) - p_0 * \left(\frac{a^2}{a^2-b^2}\right) * (1 - \frac{b^2}{r^2}) \tag{6.58}$$

$$\sigma_\theta = p_i * \frac{b^2}{a^2-b^2} * \left(1 + \frac{a^2}{r^2}\right) - p_0 * \left(\frac{a^2}{a^2-b^2}\right) * (1 + \frac{b^2}{r^2}) \tag{6.59}$$

where σ_r is the radial stress, σ_Θ is the tangential stress, p_i is the internal pressure, p_0 is the external pressure, a is the outer radius and b is the inner radius. With given loading conditions the maximum stress will be found at the inner diameter where $r=b$ [34]. To find the max stress due to the external pressure the Lamé solution then simplifies to

$$\sigma_r = -p_0 * \left(\frac{a^2}{a^2-b^2}\right) * (1 - 1) = 0 \tag{6.60}$$

$$\sigma_\theta = -p_0 * \left(\frac{a^2}{a^2-b^2}\right) * (1 + 1) = -2 * p_0 * \left(\frac{a^2}{a^2-b^2}\right) \tag{6.61}$$

Now that the stress is known, a failure criteria needs to be chosen to determine if the material will fail. The maximum shear stress criteria is used to determine the maximum allowable stress. The maximum shear stress criteria follows as

$$\tau_{max} = \frac{(\sigma_1 - \sigma_3)}{2} \tag{6.62}$$

where σ_1 is the maximum principle stress and σ_3 is the minimum principle stress. Using Equations 6.61 and 6.62 the maximum shear is determined to be

$$\tau_{max} = p_0 * \left(\frac{a^2}{a^2 - b^2}\right) \tag{6.63}$$

Copper has a shear strength 260 MPa. When τ_{max} is set to 260 MPa a maximum pressure of 195 MPa results from Equation 6.63.

When the 1C collet grips the electrode the closing force is distributed around the electrode. The 1C collet has three splits allowing for deformation of the collet. The collet does not produce hydrostatic loading but rather applies pressure to three sections of the electrode where the collet makes contact. The gripping force is applied to each of the three sections of the collet which produces pressure on the electrode. It is estimated that the maximum hydrostatic pressure of 195 MPa can be supported by each section of the electrode. With this assumption made the max gripping force is determined to be 308 N.

Since the loading is not hydrostatic but rather in three separated sections it is anticipated that the stress resulting from the applied pressure will be higher than that seen in hydrostatic loading due to presence of additional moments. For this reason the max gripping force is multiplied by a factor of 2/3. This produces a maximum gripping force of 205 N.

The gripping force is higher than the draw force of the collet due to the mechanical advantage of the collet's design. The grip force ratio for the 1C collet is 1.7:1. This allows for a maximum draw force of 120 N. The closer provides up to 273 N

of draw using the light spring and is more than enough to yield the electrode even with frictional losses in the o-ring guides and draw bar.

Since the above approximation makes some major assumptions a finite element analysis (FEA) is performed to verify the results. The finite element analysis was performed using Solidworks Simulation. The finite element analysis yields a maximum gripping stress of 125 MPa. Figure 6.4 demonstrates the stress distribution in the electrode tube. Using the results from the finite element analysis it was determined that the maximum draw force of the 1C collet when using the Copper electrode is 116 N. This result is similar to that found from previous analysis and adds confidence in the results.

6.9 Min/Max Gripping Force of Microcollet

Now that it has been shown that the 1C collet can provide more than enough gripping force the microcollet needs to be investigated to estimate the stress created in

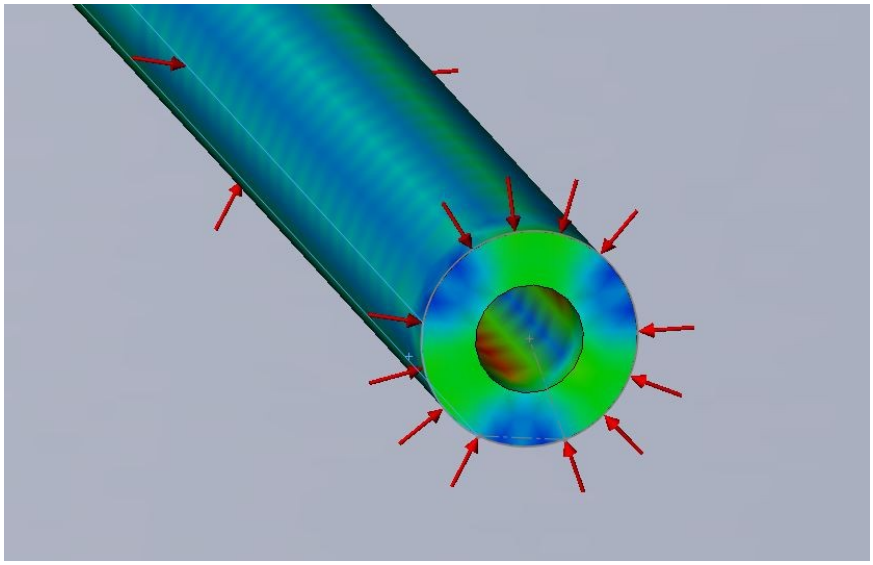

Figure 6.4: FEA results for stress in tubular electrode

the electrode. The 1C closing force is independent of the other features of the spindle, however, the closing force of the microgripper is dependent on the hydraulic pressure of the dielectric fluid. The stress developed by the microgripper needs to be determined so that the minimum and maximum dielectric pressures can be set. To begin the analysis a free body diagram of the microcollet is created. Figure 6.5 depicts the free body diagram. F is the force applied to the microcollet from the dielectric pressure forcing the gripper closing collar down. The collet is then pressed into the 30 degree closing taper in the gripper collet lid resulting in the normal force N. The friction between the surface of the collet and collet lid is also accounted for and represented by *f*. *Nx* and *Ny* are the horizontal and vertical components of N. The friction *f* is determined from the following equation

$$f = N * \mu_k \tag{6.64}$$

where μ_k is the coefficient of kinetic friction between the two steel surfaces. The equations of static equilibrium are used to solve for the unknown forces in the free body

Figure 6.5: Free body diagram of micro collet leg

diagram. The equilibrium of forces in the *x* direction follows as

$$\sum F_x = 0 = F - N * sin30° - fcos30° \tag{6.65}$$

Equation 6.65 can be used to solve for *Ny,* which is the vertical component of *N* and the gripping force of the microgripper. A solution to *Ny* follows as

$$Ny = Ncos30° = \frac{F*cos30°}{(sin30° + 0.6*cos30°)} \tag{6.66}$$

The microcollet has six splits and works by deflecting the six legs of the collet inward onto the electrode. The deflection is produced by bending the legs with the vertical component of the normal force *Ny*. The deflection of the collet legs can be calculated using Equation 6.67 which follows as

$$\delta_y = \frac{-N_y * l^3}{3*E*I} \tag{6.67}$$

where δ_y is the deflection of the free end of the collet leg and *l* is the length of the leg. The length of the microcollet leg is 3.8 mm. The moment of inertia *I* of the leg is determined using Solidworks and was found to be 0.0066mm^4.

The minimum closing force of the microcollet depends on the clearance between the collet and the electrode. Some clearance is required for the electrode to pass through freely when the collet is open. The microcollet is designed to have in inner diameter of 0.30 mm when the collet is open. This provides a clearance of 0.025 mm around the electrode. The minimum force required to close onto the electrode then follows as

$$0.025 = \frac{\left(\frac{F_{min}*cos30°}{(sin30°+0.6*cos30°)}\right)*l^3}{3*E*I} \tag{6.68}$$

Equation 6.68 is then solved for the minimum closing force F_{min}. Equation 6.68 yields a minimum closing force for each leg to be 2.049 N. Since there are six legs the combined minimum closing force becomes 12.3 N. The closing force also needs to overcome the force provided by the gripper release spring and thus the minimum closing force becomes 15.7 N. The required minimum dielectric pressure then becomes 238 psi.

The minimum dielectric pressure to close the microcollet has been determined and now the maximum dielectric pressure needs to be found. This is the pressure that will cause the copper electrode to be crushed by the microcollet. The analysis of the max closing force of the microcollet is much like that of the 1C collet. The maximum hydrostatic pressure of 125 MPa is used. This pressure is applied by each section of the microcollet and F_{max} will be the required force to provide this contact pressure. The maximum allowable dielectric pressure to not permanently deform the copper electrode is 750 psi which presses down on the microcollet with 49.3 N. The spindle is designed to be able to provide 1000 psi which is above the maximum allowable pressure for use with a copper electrode. Care must be taken when adjusting the dielectric pressure when using copper electrodes. If 750 psi does not provide a high enough exit velocity then shorter electrode lengths should be selected.

6.10 Deflection of YZ Adjust

When aligning the spindle into a machine platform the YZ adjust is elastically deformed. In order to ensure that the YZ adjust will be compliant enough to be easily deformed, a finite element analysis was performed. The analysis determined the required force to close the gap of the YZ adjust by deforming the free end 2.3mm. The analysis shows that only a 170 N force applied at the free end of the YZ adjust will produce the

needed deflection. The deflection can be seen in Figure 3.33. When deflecting the YZ adjust there is a high stress concentration in the thin section of material that serves as the pivot when flexing. In order to ensure that the part will not fail the finite element analysis also used to provide the stress levels in this region. The analysis shows that the yield stress for the material is reached just as the 2.3mm of deflection is reached. Figure 6.6 shows the stress results of the finite element analysis at 2.3mm deflection.

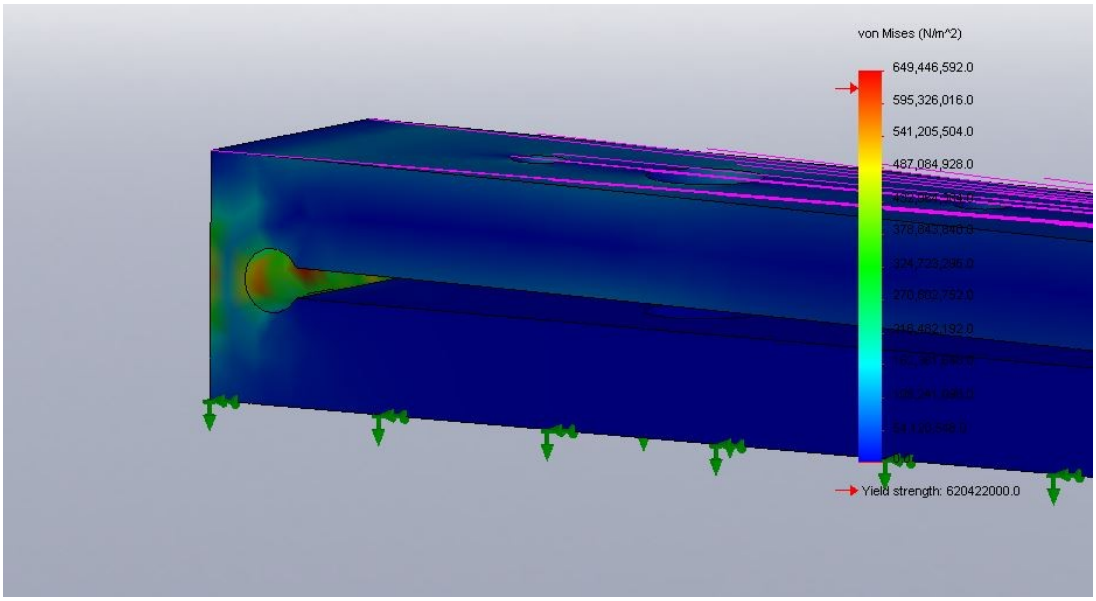

Figure 6.6: FEA results for stress in YZ adjust

CHAPTER 7

CONCLUSION

Technological advancements such as the smart phone, which allows us to carry an incredibly small and powerful computer around in our pocket, are dependent upon the ability to manufacture small and complex components. Many of these components are made of hard-to-machine materials or come from hard and complex micro molds. In either case, the electric discharge milling process is well suited to meet the demands of precision micro machining. Not only are computers becoming smaller, but the medical and optical industries are rapidly evolving, requiring evermore complex mechanisms with small and hard-to-machine features. The manufacturing industry needs to keep pace in order to support the development of these new technologies that enhance our everyday lives.

The microelectric discharge milling spindle design presented in this thesis offers a compact, versatile, and economical solution to the challenges of micro machining. The spindle offers the ability to use a wide range of electrode sizes and shapes using an industrial standard collet. The ability to also load long electrodes promotes long machining intervals without operator interaction. The spindle offers optimum flushing of the dielectric fluid for a wide range of machining applications. The unique design offers variable dielectric fluid pressure to ensure a constant exit velocity from the electrode. The spindle is also designed to be dipped into a tank so that immersion flushing may be

utilized. The dielectric fluid chosen for the spindle design optimizes the machining process and enhances operator safety. The spindle's unique C-axis capability enables the creation of a variety of electrode shapes which can be used for sinking operations. The spindle's design also promotes simple adaptation into a multitude of CNC machine platforms, including 4- and 5-axis machines. The spindle's deep hole guide also provides the ability to drill deep micro holes when integrated into a machining platform.

The advantages of this spindle design should make it a powerful tool in the creation of microcomponents. Prototyping and testing of the design is now required so that further developments of the design can continue.

REFERENCES

[1] Chung D. K.; Kim B. H.; Chu C. N. Micro electrical discharge milling using deionized water as a dielectric fluid. *Journal of Miromechanics and Microengineering* **2007**, *17*, 867-874.

[2] Bamberg E.; Heamawatanachai S. Orbital electrode actuation to improve efficiency of drilling micro-holes by micro-edm. *Journal of Materials Processing Technology* **2009**, *209*, 1826-1834.

[3] Masuzawa T.; Fujino M.; Kobyashi K.; Suzuki T.; Kinoshita N. Wire electro-discharge grinding for micro-machining. *CIRP Ann.* **1985**, *34,* 431-434.

[4] Liu K.; Lauwers B.; Reynaerts D. Process capabilities of mico-edm and its applications. *International Journal of Advanced Manufacturing Technology* **2010**, *47*, 11-19.

[5] Pham D. T.; Dimov S. S.; Bigot S.; Ivanov A.; Popov K. (2004). Micro-edm-recent developments and research issues. *Journal of Materials Processing Technology* **2004**, *147*, 50-57

[6] Fleischer J.; Masuzawa T.; Schmidt J.; Knoll M. New applications for micro-edm. *Journal of Materials Processing Technology* **2004**, *149*, 246-249

[7] Chen S. T.; Yang H. Y. Study on ultra-fine w-edm with on-machine measurement-assisted. In *International Conference on Advances in Materials and Processing Technologies*; Chinesta, F.; El Mansori, M., Eds.; AIP Conference Proceedings Series 1315; American Institute of Physics: 2010; pp. 1255-1260

[8] Chern G. L.; Wu Y. E.; Cheng J. C.; Yao J. C. Study on burr formation in micro-machining using micro-tools fabricated by micro-edm. *Precision Engineering* **2007**, *31*, 122-129

[9] Bleys P.; Kruth J. P.; Lauwers B. (2004). Sensing and compensation of tool wear in milling edm. *Journal of Materials Processing Technology* **2004**, *149*,139-146.

[10] Lin C. T.; Chow H. M.; Yang L. D.; Chen Y. F. Feasibility study of micro-slit edm machining using pure water. *International Journal of Advanced Manufacturing Technology* **2007**, *34*, 104-110.

[11] Richter, A. Dielectric fluids for micro-edming. *MICROmanufacturing* **2011**, *4(2),* 1-3.

[12] Kibria G.; Sarkar B. R.; Pradhan B. B.; Bhattacharyya B. (2010). Comparative study of different dielectrics for micro-edm performance during microhole machining of Ti-6Al-4V alloy. *International Journal of Advanced Manufacturing Technology* **2010**, *48*, 557-570.

[13] Liu Y. H.; Ji R. J.; Li X. P.; Yu L. L.; Zhang H. F.; Li Q. Y. Effect of machining fluid on the process performance of electric discharge milling of insulating Al_2O_3 ceramic. *International Journal of Machine Tools & Manufacturing* **2008**, *48*, 1030-1035.

[14] Jameson, Elman C. *Electrical Discharge Machining*; Society of Manufacturing Engineering: Michigan, 2001, pp 159-210.

[15] Guitrau, E. Bud. *The EDM Handbook;* Hanser: Cincinnati, 2009; pp 57-63, 192-196, 227-231.

[16] Sommer C.; Sommer S. *Complete EDM Handbook*. Advance Publishing: Houston, 2005; pp 157-189.

[17] Meena V. K.; Azad M. S.; Mitra S. Effect of flushing condition on deep hole micro-edm drilling. *International Journal of Machining and Machinability of Materials* **2012**, *12(4),* 308-320.

[18] Mohan B.; Rajadurai A.; Satyanarayana K. G. Electric discharge machining of Al-SiC metal matrix composites using rotary tube electrode. *Journal of Materials Processing Technology* **2004**, *153-154*, 978-985.

[19] Wang Y.; Bai J.; Guo Y.; Huang H. Investigation of the effects of dielectric inlet pressure in inner jetted dielectric EDMmilling. *Advanced Materials Research* **2011**, *189-193*, 125-128.

[20] Karthikeyan G.; Ramkumar J.; Dhamodaran S.; Aravindan S. Micro electric discharge milling process performance: an experimental investigation. *International Journal of Machine Tools & Manufacture* **2010**, *50*, 718-727

[21] Kuppan P.; Rajadurai A.; Narayanan. Influence of edm process parameters in deep hole drilling of inconel. *International Journal of Manufacturing Technology* **2008**, *718 38*, 74-84

[22] Wikipedia. *End Face Mechanical Seal*, www.wikipedia.org (accessed July 26, 2013).

[23] Rotary Systems Inc. *Series 008 High Speed Air/Hydraulic Rotary Union*, www.rotarysystems.com (accessed June, 2013).

[24] Tescom, *ER3P Series Kit I or Kit II*, www.tescom.com (accessed September, 2013).

[25] *Parker O-Ring Handbook* [Online]; Parker Hannifin Corp.: Cleveland, OH, 2007: pp.126-292. http://www.parker.com/portal/site/PARKER/menuitem.734d2913eb3c11da13576f849420d1ca/?vgnextoid=d195f87357e28110VgnVCM10000048021dacRCRD&vgnextfmt=EN&lit=Catalogs&ky=4f85a0a86f91d110VgnVCM10000032a71dacRCRD&kyEN=Seals&iden=&stpoint=K&fromSource=&fromId=&openurl=url# (accessed June, 2013).

[26] SKF. *Rolling Bearing Catalog*, www.skf.com (accessed July, 2013).

[27] MIT Precision Engineering Research Group. *Fundamentals of Design Topic 10 Bearings*, http://pergatory.mit.edu/resources/FUNdaMENTALS.html (accessed August, 2013).

[28] Oberg, E.; Jones, Franklin D.; Horton, Holbroock L.; Ryffel Henry H. *Machinery's Handbook, Twenty-Seventh Edition;* Industrial Press: New York, 2004

[29] SKF. *High Performance Hybrid Bearings for Increased Spindle Performance*, www.skf.com. [30] Fox, Robert J.; McDonald, Alan T.; Pritchard, Philip J. *Introduction to Fluid Mechanics, Sixth Edition;* John Wiley & Sons: Danvers, 2006, pp 41-45, 263-271, 317-352.

[31] Hibbeler, R.C. *Mechanics of Materials, Fifth Edition;* Pearson Education Inc.: Upper Saddle River, 2003.

[32] Boresi; Arthur P.; Schmidt, Richard J. *Advanced Mechanics of Materials, Sixth Edition*; John Wiley and Sons: Danvers, 2003, pp 178-185, 381.

[33] Automation Direct. *Encoder Frequently Asked Questions*. www.automationdirect.com (accessed November, 2013).

[34] Cook, Robert D.; Young, Warren C. *Advanced Mechanics of Materials, Second Edition*, Prentice Hall Inc.: Upper Saddle River, 1999, pp 94-102